

# Rényi entropies after releasing the Néel state in the XXZ spin-chain

Vincenzo Alba and Pasquale Calabrese

International School for Advanced Studies (SISSA), Via Bonomea 265, 34136, Trieste, Italy, INFN, Sezione di Trieste

## Abstract.

We study the Rényi entropies in the spin-1/2 anisotropic Heisenberg chain after a quantum quench starting from the Néel state. The quench action method allows us to obtain the stationary Rényi entropies for arbitrary values of the index  $\alpha$  as generalised free energies evaluated over a calculable thermodynamic macrostate depending on  $\alpha$ . We work out this macrostate for several values of  $\alpha$  and of the anisotropy  $\Delta$  by solving the thermodynamic Bethe ansatz equations. By varying  $\alpha$  different regions of the Hamiltonian spectrum are accessed. The two extremes are  $\alpha \rightarrow \infty$  for which the thermodynamic macrostate is either the ground state or a low-lying excited state (depending on  $\Delta$ ) and  $\alpha = 0$  when the macrostate is the infinite temperature state. The Rényi entropies are easily obtained from the macrostate as function of  $\alpha$  and a few interesting limits are analytically characterised. We provide robust numerical evidence to confirm our results using exact diagonalisation and a stochastic numerical implementation of Bethe ansatz. Finally, using tDMRG we calculate the time evolution of the Rényi entanglement entropies. For large subsystems and for any  $\alpha$ , their density turns out to be compatible with that of the thermodynamic Rényi entropies.

## 1. Introduction

The extraordinary progress in the field of ultracold atomic gases provided the unprecedented opportunity to observe experimentally the real time dynamics of isolated many-body quantum systems [1–10]. The theoretical laboratory for studying this fascinating physical phenomenon is the quantum quench, in which a system is prepared in a pure state  $|\Psi_0\rangle$ , and it is let evolve unitarily under the action of a many-body Hamiltonian  $H$ . Relevant questions that have been addressed so far include what is the nature of the steady state arising at infinite time and whether it is possible to describe it using the paradigm of thermalization [11–17]. It is nowadays well established that integrable systems fail to thermalise, contrary to non-integrable ones, because of the presence of relevant conservation laws constraining their dynamics at any time. It has been recognised that local properties in the steady state are described by a Generalised Gibbs Ensemble (GGE) [18–49], which is obtained by supplementing the Gibbs ensemble with the additional local and quasi-local conserved quantities of the model [50].

However, unitarity of the time evolution in quantum mechanics implies that a quenched system can never relax as a whole to a statistical ensemble with non zero entropy. Thus equilibration and thermalisation must be intended at the level of subsystems. Given a finite compact subsystem  $A$  embedded in an infinite system, its time dependent reduced density matrix is  $\rho_A(t) \equiv \text{Tr}_{\bar{A}}|\Psi(t)\rangle\langle\Psi(t)|$ , where the trace is over  $\bar{A}$ , the complement of  $A$ . The reduced density matrix  $\rho_A(t)$  generically corresponds to a mixed state with non-zero entropy which is known as entanglement entropy [51]. The reduced density matrix can have a well defined infinite time limit  $\rho_A(\infty)$  with non-zero entropy density. A stationary state is described by a statistical ensemble with density matrix  $\rho_E$  for the entire system, if its reduced density matrix  $\rho_{A,E} = \text{Tr}_{\bar{A}}(\rho_E)$  equals  $\rho_A(\infty)$  [20, 21, 26, 32, 48]. According to this logic, it is natural that the extensive thermodynamic entropy of the statistical ensemble is nothing but the entanglement accumulated in time<sup>‡</sup>.

The entropy of a (reduced) density matrix  $\rho$  is traditionally measured by the von Neumann form

$$S[\rho] \equiv -\text{Tr}\rho \ln \rho, \quad (1)$$

but recently alternative measures like the Rényi entropies

$$S^{(\alpha)}[\rho] \equiv \frac{1}{1-\alpha} \ln \text{Tr}\rho^\alpha, \quad (2)$$

are becoming more and more popular. In the limit  $\alpha \rightarrow 1$  one has  $S^{(\alpha)} \rightarrow S$ , but the knowledge of the Rényi entropies for different values of the index  $\alpha$  gives access to much more information than the von Neumann entropy alone, as for example the entire spectrum of the density matrix (see e.g. [52]). Furthermore, Rényi entropies for integer  $\alpha$  are the essence of the replica approach to the entanglement entropy [53]. While the

<sup>‡</sup> In this paper, two entropies are the same when they have the same extensive behaviour, i.e. when their densities are equal. They can have different subleading terms, and in most cases they do.

replica method was introduced mainly as a theoretical analytic tool to deal with the complexity of  $\rho_A$  [53], it became a fundamental idea to access the entanglement entropy in stochastic numerical simulations based on Monte Carlo [54] and in experiments: Rényi entanglement entropies (for  $\alpha = 2$ ) have been measured experimentally with cold atoms, both in equilibrium [55] and after a quantum quench [10].

The equivalence between stationary entanglement entropy  $S_A(\infty) \equiv S[\rho_A(\infty)]$  (of a finite subsystem  $A$  of volume  $V_A$  embedded in an infinite system) and thermodynamic entropy  $S_E \equiv S[\rho_E]$  (of a large system of volume  $V$ ) implies that

$$\lim_{V_A \rightarrow \infty} \frac{S_A(\infty)}{V_A} = \lim_{V \rightarrow \infty} \frac{S_E}{V}. \quad (3)$$

This equivalence has been very recently exploited to give an analytic exact prediction for the entire time dependence of the entanglement entropy in integrable models [56] as also carefully tested against numerical simulations in the XXZ spin-chain [56]. Obviously Eq. (3) is valid also for the Rényi entropies (2) and it is natural to wonder if and how the results of [56] generalise to these entropies.

At the same time, another interesting entropy for a non equilibrium quantum system is the diagonal entropy  $S_d$  [57], which is the von Neumann entropy of the diagonal ensemble with density matrix

$$\rho_d = \sum_{m=1}^{\infty} w_m |m\rangle\langle m| \quad \text{with} \quad w_m \equiv |\langle \Psi_0 | m \rangle|^2, \quad (4)$$

where  $|m\rangle$  denotes a generic eigenstate of  $H$  and  $w_m$  its overlap with the initial state. In terms of (4), the diagonal Rényi entropies  $S_d^{(\alpha)}$  are

$$S_d^{(\alpha)} \equiv \frac{1}{1-\alpha} \ln \text{Tr} \rho_d^\alpha = \frac{1}{1-\alpha} \ln \sum_m w_m^\alpha, \quad (5)$$

and of course the diagonal entropy  $S_d = -\text{Tr} \rho_d \ln \rho_d$  can be obtained in the limit  $\alpha \rightarrow 1$ . The diagonal entropies have the great advantage that can be very easily calculated even for finite systems and without the need of solving the many-body dynamics. For this reason, a lot of effort has been devoted to understand the relation between the diagonal entropy and the thermodynamic one, i.e. the stationary subsystem entanglement entropy, see e.g. [58–67]. It has been suggested that for integrable models, the diagonal von Neumann entropy is half the thermodynamic entropy [59,60], a relation that has been proved only recently [68] for a precise class of initial states. Furthermore it has been also shown [68] that, for this specific class of initial states, the ratio of entropies is equal to 1/2 not only for the von Neumann ones, but in general for Rényi entropies of arbitrary order. It has been subsequently found [69] that some initial states with peculiar symmetries exist such that the ratio between these two entropies is different from 1/2. However, these states have been explicitly constructed only for non-interacting systems and it is unclear whether the result generalises to interacting models (see also [70]).

The main goal of this paper is to continue the investigation of the Rényi entropies after a quench initiated in [68]. A first objective will be to substantiate the general results of [68] with an accurate analytic and numerical analysis of the Rényi entropies for a very

specific quench: the time evolution of the anisotropic XXZ spin-chain starting from the Néel state. A second one is to study numerically the entanglement Rényi entropies by means of tDMRG to start making a connection with the quasiparticle picture [71, 72] used for the von Neumann entropy in [56].

The technique we will use to compute the Rényi entropy is the one introduced in [68], which is an adaptation of the Thermodynamic Bethe Ansatz (TBA) approach to quantum quenches (overlap TBA or Quench Action method [73, 74]). This technique provides an analytic machinery to compute the Rényi entropies both of the diagonal ensemble and of the GGE. Within this approach, in the thermodynamic limit,  $S_d^{(\alpha)}$  is given as a generalised free energy

$$S_d^{(\alpha)} = \frac{1}{\alpha - 1} \left( 2\alpha\mathcal{E} - \frac{1}{2}S_{YY} \right) \Big|_{\rho_\alpha^*}. \quad (6)$$

Here  $S_{YY}$  is the Yang-Yang entropy [75] and  $\mathcal{E} \equiv -2\ln|w_m|$  is the strength of the overlap (4) between the eigenstates of the chain and the initial state. This form is valid for a specific class of initial states which have non-zero overlap only with parity invariant Bethe states, as most of the quenches solved so far [76–85] (see however [69]). In Ref. [68] it has also been shown that after some algebraic manipulations, the Rényi entropies of the GGE corresponding to the stationary state can be rewritten as

$$S_{\text{GGE}}^{(\alpha)} = \frac{1}{\alpha - 1} \left( 4\alpha\mathcal{E} - S_{YY} \right) \Big|_{\rho_\alpha^*}, \quad (7)$$

showing that  $S_{\text{GGE}}^{(\alpha)} = 2S_d^{(\alpha)}$  for generic  $\alpha$ . In (6) and (7),  $\rho_\alpha^*$  identifies a saddle point eigenstate (representative eigenstate or thermodynamic macrostate) of the XXZ chain. It turned out that  $\rho_\alpha^*$  in (6) depends on the Rényi index  $\alpha$ , and it is not the macrostate describing the local observables and the von Neumann entropy [56], which is recovered only for  $\alpha = 1$ . This implies that, for generic  $\alpha$ ,  $S_{YY}$  in (6) is not the thermodynamic entropy of the GGE. An intriguing consequence of this finding is that the steady state contains information about different regions of the spectrum of the XXZ chain, which can be accessed by varying  $\alpha$ . This is similar, in spirit, to the observation of Ref. [86] that a single eigenstate of a generic (non-integrable) Hamiltonian at finite energy density contains information about the full spectrum of the Hamiltonian.

The paper is organised as follows. Section 2 introduces the XXZ chain, the quench protocol and the Bethe ansatz solution, focusing on the TBA formalism (subsection 2.2). In section 3 we illustrate the TBA calculation of the Rényi diagonal and GGE entropies and in Section 4 we present a few limits that can be worked out analytically. Section 5 reports the results for the Rényi entropies for general values of  $\alpha$ ; numerical checks are also presented in this section using exact diagonalisation (subsection 5.2.1) and a stochastic numerical implementation of the Bethe ansatz for finite systems (subsection 5.2.2). Finally, in section 6 we numerically evaluate the Rényi entanglement entropies and extrapolate to infinite subsystem size to confirm that they have the same density as the thermodynamic GGE entropies. In the conclusions (section 7) we summarise our findings and discuss some possible future directions.

## 2. Model, quench & Bethe ansatz solution

We consider quantum quenches in the spin-1/2 anisotropic Heisenberg chain (XXZ chain) defined by the Hamiltonian

$$H = \sum_{i=1}^L \left[ \frac{1}{2} (S_i^+ S_{i+1}^- + S_i^- S_{i+1}^+) + \Delta \left( S_i^z S_{i+1}^z - \frac{1}{4} \right) \right], \quad (8)$$

where  $S_i^\alpha$  are spin-1/2 operators, and  $\Delta$  is the anisotropy. We use periodic boundary conditions, identifying sites 1 and  $L+1$  of the chain. We restrict ourselves to  $\Delta \geq 1$ . For any  $\Delta$ , the XXZ Hamiltonian (8) commutes with the total magnetisation  $S_T^z \equiv \sum_i S_i^z$ . Due to the periodic boundary conditions, (8) is invariant under one-site translations  $S_i^\alpha \rightarrow S_{i+1}^\alpha$ , i.e.,  $[\mathcal{T}, H] = 0$ , with  $\mathcal{T}$  the translation operator. The XXZ model is also invariant under reflections with respect to the center of the chain, i.e.,  $S_i^\alpha \rightarrow S_{L-i+1}^\alpha$ , implying that  $[\mathcal{P}, H] = 0$ , with  $\mathcal{P}$  the parity operator. As a consequence, in the numerical analysis it is convenient to label the eigenstates of (8) as  $|s_T^z, k, p\rangle$ , with  $s_T^z, k, p$  the eigenvalues of  $S_T^z, \mathcal{T}, \mathcal{P}$ .

In the following, we consider the quench from the Néel state  $|N\rangle \equiv |\uparrow\downarrow\uparrow\downarrow\cdots\rangle = |\uparrow\downarrow\rangle^{\otimes L/2}$ . To exploit translation invariance, we consider the combination

$$|\Psi_0\rangle = \frac{|N\rangle + |\bar{N}\rangle}{\sqrt{2}}, \quad (9)$$

where  $|\bar{N}\rangle \equiv |\downarrow\uparrow\rangle^{\otimes L/2}$  denotes the anti-Néel state. At time  $t = 0$  the chain is prepared in the state  $|\Psi_0\rangle$ , and the subsequent dynamics is generated by (8). Crucially,  $|\Psi_0\rangle$  is invariant under all the symmetries of (8), i.e.,  $\mathcal{S}|\Psi_0\rangle = |\Psi_0\rangle$  for  $\mathcal{S} = S_T^z, \mathcal{T}, \mathcal{P}$ . Thus, only the eigenstates of (8) with  $s_T^z = k = 0$  and  $p = +1$  can have non zero overlap with the state (9). We anticipate (see subsection 5.2.1) that using these symmetries in exact (full) diagonalisation allows us to obtain all the eigenstates with non-zero Néel overlap for a chain with  $L \approx 22$  sites.

### 2.1. Bethe ansatz solution of the XXZ chain

The XXZ chain is exactly solvable by Bethe ansatz [87]. In the Bethe ansatz solution, the eigenstates of (8) in the sector with  $M$  down spins (particles), i.e., with fixed total magnetisation  $S_T^z = L/2 - M$ , are in correspondence with a set of  $M$  rapidities  $\lambda_j \in \mathbb{C}$ . These are obtained by solving the Bethe equations

$$\left[ \frac{\sin(\lambda_j + i\frac{\eta}{2})}{\sin(\lambda_j - i\frac{\eta}{2})} \right]^L = - \prod_{k=1}^M \frac{\sin(\lambda_j - \lambda_k + i\eta)}{\sin(\lambda_j - \lambda_k - i\eta)}, \quad (10)$$

where  $\eta \equiv \text{arccosh}(\Delta)$ . The corresponding eigenstate energy  $E$  is given in terms of the rapidities as

$$E = - \sum_{i=1}^M \frac{\sinh^2 \eta}{\cosh \eta - \cos(2\lambda_i)}. \quad (11)$$

In the thermodynamic limit the solutions (10) form string patterns in the complex plane. Here the thermodynamic limit  $\lim$  is taken with the number of particles (flipped spins)  $N$  and the length  $L$  going to infinity at fixed density  $N/L$ . The rapidities forming a  $n$ -string, with  $n$  being the string length, can be parametrised as [87]

$$\lambda_{n,\gamma}^j = \lambda_{n,\gamma} + i\frac{\eta}{2}(n+1-2j) + \delta_{n,\gamma}^j, \quad (12)$$

where  $j = 1, \dots, n$  labels the different string components,  $\lambda_{n,\gamma} \in \mathbb{R}$  is the “string center”, and  $\delta_{n,\gamma}^j$  are the string deviations. For most of the eigenstates of (8),  $\delta_{n,\gamma}^j = \mathcal{O}(e^{-L})$ , allowing one to neglect the string deviations [87] (string hypothesis). Physically,  $n$ -strings describe bound states of  $n$  down spins. The string centres  $\lambda_{n,\gamma}$  are obtained by solving the Bethe-Gaudin-Takahashi (BGT) equations [87]

$$L\theta_n(\lambda_{n,\gamma}) = 2\pi I_{n,\gamma} + \sum_{(n,\gamma) \neq (m,\beta)} \Theta_{n,m}(\lambda_{n,\gamma} - \lambda_{m,\beta}). \quad (13)$$

Here  $I_{n,\gamma} \in \frac{1}{2}\mathbb{Z}$  are the BGT quantum numbers and  $\Theta_{n,m}$  the scattering phases between different string types

$$\Theta_{n,m}(\lambda) \equiv (1 - \delta_{n,m})\theta_{|n-m|}(\lambda) + 2\theta_{|n-m|+2}(\lambda) + \dots + \theta_{n+m-2}(\lambda) + \theta_{n+m}(\lambda). \quad (14)$$

Each different choice of quantum numbers  $I_{n,\gamma}$  gives different sets of solutions of (13), i.e., a different eigenstate of (8). For  $\Delta > 1$ , one has  $\lambda_{n,\gamma} \in [-\pi/2, \pi/2)$ . In (13) we define  $\theta_n(\lambda) \equiv 2 \arctan[\tan(\lambda)/\tanh(n\eta/2)]$ . The eigenstate energy  $E$  and its total momentum  $K$  are obtained by summing over the rapidities as

$$E = \sum_{n,\gamma} \epsilon_n(\lambda_{n,\gamma}), \quad \text{with} \quad \epsilon_n(\lambda) \equiv -\frac{\sinh(\eta) \sinh(n\eta)}{\cosh(n\eta) - \cos(2\lambda)}, \quad (15)$$

$$K = \sum_{n,\gamma} z_n(\lambda_{n,\gamma}), \quad \text{with} \quad z_n(\lambda_{n,\gamma}) = \frac{2\pi I_{n,\gamma}}{L}. \quad (16)$$

In the following, we will also consider the XXX chain, which is obtained by setting  $\Delta = 1$  in (8). Bethe ansatz results for the XXX chain can be obtained from those for the XXZ model by taking an appropriate scaling limit. One first rewrites the formulas for the XXZ chain in terms of the rescaled rapidities  $\mu$  defined as

$$\mu \equiv \frac{\lambda}{\eta} \quad \text{with} \quad \eta \equiv \operatorname{arccosh} \Delta. \quad (17)$$

Since  $\eta \rightarrow 0$  for  $\Delta \rightarrow 1$ , the rescaled rapidities  $\mu$  are defined in the interval  $[-\infty, \infty]$ . Also, from (12) one has that the spacing between string components along the imaginary axis becomes  $i/2$ . Finally, the limit  $\eta \rightarrow 0$  has to be taken. For instance, using (15), for the XXX chain  $\epsilon_n$  becomes

$$\epsilon_n(\mu) = \frac{2n}{4\mu^2 + n^2}. \quad (18)$$

## 2.2. Thermodynamic Bethe ansatz (TBA)

In the thermodynamic limit the solutions of the BGT equations (13) become dense on the real axis. Local properties of the system can be extracted from the rapidity densities  $\rho_n(\lambda)$  (one for each string type), which are formally defined as

$$\rho_n(\lambda) \equiv \lim_{L \rightarrow \infty} \frac{1}{L(\lambda_{n,\gamma+1} - \lambda_{n,\gamma})}. \quad (19)$$

To characterise the thermodynamic state of the system one also needs the densities  $\rho_n^{(h)}(\lambda)$  of the  $n$ -string holes, i.e., of the unoccupied string centres and it is also custom [87] to introduce the total densities  $\rho_n^{(t)}(\lambda) \equiv \rho_n(\lambda) + \rho_n^{(h)}(\lambda)$ .

The  $\rho_n^{(h)}(\lambda)$  and  $\rho_n(\lambda)$  are related via the thermodynamic version of the BGT equations

$$\rho_n^{(h)}(\lambda) + \rho_n(\lambda) = a_n(\lambda) - \sum_{m=1}^{\infty} (a_{nm} \star \rho_m)(\lambda), \quad (20)$$

which are obtained from (13) by taking the thermodynamic limit. In (20) we defined  $a_{nm}(\lambda)$  as

$$a_{nm}(\lambda) = (1 - \delta_{nm})a_{|n-m|}(\lambda) + 2a_{|n-m|}(\lambda) + \dots + 2a_{n+m-2}(\lambda) + a_{n+m}(\lambda), \quad (21)$$

where

$$a_n(\lambda) = \frac{1}{\pi} \frac{\sinh(n\eta)}{\cosh(n\eta) - \cos(2\lambda)}. \quad (22)$$

The convolution  $f \star g$  between two functions is defined as

$$(f \star g)(\lambda) = \int_{-\pi/2}^{\pi/2} d\mu f(\lambda - \mu)g(\mu). \quad (23)$$

Thus in the thermodynamic limit, the total magnetisation and energy densities become

$$\frac{S_T^z}{L} = \sum_{n=1}^{\infty} n \int_{-\pi/2}^{\pi/2} d\lambda \rho_n(\lambda), \quad (24)$$

$$\frac{E}{L} = \sum_{n=1}^{\infty} \int_{-\pi/2}^{\pi/2} d\lambda \epsilon_n(\lambda) \rho_n(\lambda), \quad (25)$$

where  $\epsilon_n(\lambda)$  is defined in (15). The set of root densities  $\boldsymbol{\rho} \equiv \{\rho_n\}_{n=1}^{\infty}$  defines a thermodynamic macrostate, and it allows to obtain the expectation values of local or quasi-local observables in the thermodynamic limit. A thermodynamic macrostate corresponds to an exponentially large (with  $L$ ) number of microscopic eigenstates (microstates), which lead to the same set of rapidity densities in the thermodynamic limit. Any of the equivalent microscopic eigenstates can be chosen as a finite-size representative of the thermodynamic macrostate. The total number of equivalent microstates is  $e^{S_{YY}}$ , with  $S_{YY}$  the Yang-Yang entropy [75]

$$S_{YY}[\boldsymbol{\rho}] \equiv L \sum_{n=1}^{\infty} \int_{-\pi/2}^{\pi/2} d\lambda \left[ \rho_n^{(t)} \ln \rho_n^{(t)} - \rho_n \ln \rho_n - \rho_n^{(h)} \ln \rho_n^{(h)} \right]. \quad (26)$$

Clearly,  $S_{YY}$  is extensive. For systems in thermal equilibrium  $S_{YY}$  is the thermal entropy.

As we shall see, the TBA equations assume a more compact form in terms of the ratio

$$\eta_n(\lambda) \equiv \frac{\rho_n^{(h)}(\lambda)}{\rho_n(\lambda)}, \quad (27)$$

which we define here for later convenience.

### 3. Overlap TBA for the Rényi entropies

In this section we briefly recall the approach of Ref. [68] to calculate Rényi entropies (both for the diagonal ensemble and for the GGE) and then specialise it to the XXZ spin-chain, in particular for the quench from the Néel state. The quench action [73, 74] provides a calculable and manageable representation of the stationary state (or equivalently of the diagonal ensemble), as nowadays explicitly worked out for many integrable models [69, 79, 88–99]. Furthermore, it can also be used to study the time evolution of local observables as done in a few simple cases [100–102]. In [68] the Quench Action method has been generalised to obtain the stationary values of the Rényi entropies which are non-local quantities and indeed the approach introduces important novelties.

For the diagonal ensemble, the starting point is the thermodynamic limit of the overlaps  $w_m$  appearing in the diagonal ensemble (4) which can be written as

$$w_m = \exp(-2\mathcal{E}(m)), \quad \text{with} \quad \mathcal{E} \equiv -\lim_{\text{th}} [\text{Re}(\ln\langle m|\Psi_0\rangle)]. \quad (28)$$

In the thermodynamic limit the sum over eigenstates appearing in (4) and (5) is replaced by a functional integral over the rapidity densities as

$$\sum_m \rightarrow \int \mathcal{D}\boldsymbol{\rho} e^{S_{YY}[\boldsymbol{\rho}]}, \quad (29)$$

where the factor  $e^{S_{YY}}$ , with  $S_{YY}$  the Yang-Yang entropy (26), takes into account the exponentially large number of microscopic eigenstates leading to the same densities. In (29),  $\mathcal{D}\boldsymbol{\rho} \equiv \prod_{n=1}^{\infty} \mathcal{D}\rho_n(\lambda)$ . Using (4), (28), and (29) one obtains

$$\text{Tr}\rho_d^\alpha = \int \mathcal{D}\boldsymbol{\rho} e^{-2\alpha\mathcal{E}[\boldsymbol{\rho}] + \frac{1}{2}S_{YY}[\boldsymbol{\rho}]}. \quad (30)$$

The factor  $1/2S_{YY}$  takes into account that only parity-invariant eigenstates of (8) have non-zero overlap with the Néel state [91]. These correspond to solutions of the Bethe equations containing only pairs of rapidities with opposite sign, i.e., such that  $\{\lambda_j\}_{j=1}^M = \{-\lambda_j\}_{j=1}^M$ .

In a similar fashion, it has been shown in [68] that the Rényi GGE entropies can be written as

$$\text{Tr}\rho_{\text{GGE}}^\alpha = \int \mathcal{D}\boldsymbol{\rho} e^{-4\alpha\mathcal{E}[\boldsymbol{\rho}] + S_{YY}[\boldsymbol{\rho}]}. \quad (31)$$

It is evident that both in (30) and (31), the function  $\mathcal{E}$  acts as driving term replacing the Hamiltonian in the standard TBA at finite temperature.



In the thermodynamic limit, the path integrals (30) and (31) are dominated by the saddle point, obtained by minimising the exponent. Since the exponent in one case is just the double of the other,  $\rho_\alpha^*$  is the same in the two cases and can be obtained as solution of the saddle point equation

$$\left[ -4\alpha \frac{\delta \mathcal{E}(\rho)}{\delta \rho} + \frac{\delta S_{YY}(\rho)}{\delta \rho} \right]_{\rho=\rho_\alpha^*} = 0 \quad (32)$$

and hence the Rényi entropies are

$$S_d^{(\alpha)} = \frac{1}{1-\alpha} \left[ -2\alpha \mathcal{E}(\rho_\alpha^*) + \frac{1}{2} S_{YY}(\rho_\alpha^*) \right] = \frac{1}{2} S_{\text{GGE}}^{(\alpha)}. \quad (33)$$

Having established that the GGE entropy is just the double of the diagonal entropy, in the following we will just refer to the latter, being clear that, at this point, the former does not provide any further information.

We now are ready to specify the general approach to the quench in the XXZ spin-chain from the Néel state. The overlaps between the Néel state and the Bethe eigenstates have been derived in full generality for finite systems in [80]. The extensive part of the thermodynamic limit has been extracted analytically in [91] and it is given as

$$\mathcal{E} = \frac{L}{2} \sum_n \int_0^{\frac{\pi}{2}} d\lambda \rho_n(\lambda) [g_n(\lambda) + 4n \ln 2], \quad (34)$$

where

$$g_n = \sum_{l=0}^{n-1} \ln \left[ \frac{s_{n-1-2l} c_{n-1-2l} s_{-n+1+2l} c_{-n+1+2l}}{t_{n-2l} t_{-n+2l}} \right], \quad (35)$$

with

$$s_n(\lambda) \equiv \sin \left( \lambda + i \frac{n\eta}{2} \right), \quad (36)$$

$$c_n(\lambda) \equiv \cos \left( \lambda + i \frac{n\eta}{2} \right), \quad (37)$$

$$t_n(\lambda) = \frac{s_n(\lambda)}{c_n(\lambda)}. \quad (38)$$

Thus, the saddle point equation (32) yields the generalised TBA equations

$$\ln[\eta_n(\lambda)] = 2n[\alpha \ln 4 - h] + \alpha g_n(\lambda) + \sum_{m=1}^{\infty} a_{nm} \star \ln(1 + \eta_m^{-1})(\lambda), \quad (39)$$

which is an infinite system of coupled integral equations for  $\eta_n$ . In (39)  $a_{nm}$  are the same as in (20). The magnetic field  $h$  (a.k.a. the chemical potential) has to be introduced to ensure the zero magnetisation condition

$$\sum_{m=1}^{\infty} m \int_{-\frac{\pi}{2}}^{\frac{\pi}{2}} d\lambda \rho_m(\lambda) = \frac{1}{2}. \quad (40)$$

For all the values of  $\alpha$  that we considered, we numerically verified that for  $\Delta > 1$  the constraint (40) is satisfied.

Similar to the standard TBA [87], it is possible to partially decouple the equations for different  $n$  in the system (39). This leads to the partially decoupled equations [91]

$$\ln \eta_n = \alpha d_n + s \star [\ln(1 + \eta_{n-1}) + \ln(1 + \eta_{n+1})], \quad (41)$$

with  $\eta_0 = 0$  and

$$d_n(\lambda) \equiv (-1)^n \ln \frac{\vartheta_4^2(\lambda, \tau)}{\vartheta_1^2(\lambda, \tau)} + \ln \frac{\vartheta_2^2(\lambda, \tau)}{\vartheta_3^2(\lambda, \tau)}, \quad (42)$$

$$s(\lambda) \equiv \frac{1}{2\pi} \sum_{k=-\infty}^{\infty} \frac{e^{-2ik\lambda}}{\cosh(k\eta)}. \quad (43)$$

Here  $\vartheta_k(\lambda, \tau)$  with  $\tau \equiv e^{-2\eta}$  are the Jacobi elliptic theta functions. Notice that  $d_n(\lambda)$  only depends on the parity of  $n$ . A similar decoupling can be obtained for the TBA equations (20) for  $\rho_n$  as [87, 91]

$$\rho_n(1 + \eta_n) = s \star (\rho_{n-1}\eta_{n-1} + \rho_{n+1}\eta_{n+1}), \quad (44)$$

with the convention  $\rho_0 = \delta(\lambda)$  and  $\eta_0 = 1$ .

The solutions  $\eta_n$  of (39) are used in (20) to obtain the saddle point densities  $\boldsymbol{\rho} \equiv \{\rho_n\}_{n=1}^{\infty}$ , which plugged in (33) give the Rényi entropies. For  $\alpha = 1$ , since  $\text{Tr} \rho_d = 1$ , the saddle point is

$$S_{YY} = 4\mathcal{E}. \quad (45)$$

The coupled integral equations (39) and (20) admit a unique solution for arbitrary value of  $\alpha$ . However, while, for  $\alpha = 1$  the saddle point densities can be derived analytically [91], for generic  $\alpha$  this does not seem to be possible. It would be highly desirable to find some new tricks which would allow the solution of these equations. Anyhow, in the absence of an analytic solution we should solve these equations numerically. Although (39) and (20) are a set of infinite coupled integral equations, one can truncate the system by including the first few strings  $n \leq n_{\max}$ , with  $n_{\max}$  large enough to ensure convergence, as routinely done to solve TBA equations. A test of the convergence is provided by monitoring the magnetisation sum rule (40). We numerically find that, at least for large enough  $\Delta$ , the convergence with  $n_{\max}$  is quite fast, and reliable results can be obtained using modest values of  $n_{\max}$ . As expected, the value of  $n_{\max}$  has to be increased when approaching the isotropic limit  $\Delta \rightarrow 1$ .

Some numerical results illustrating the qualitative features of the saddle point densities, obtained by solving the coupled equations (39) and (20), are reported in Figure 1. The figure shows  $\rho_n$  and  $\eta_n$  for  $n = 1, 2$ , and Rényi index  $\alpha = 1/2, 1, 2, 3$  (different lines in the Figure). The data are for  $\Delta = 2$ . For  $\alpha = 1$  we report the analytically known solution [91]. For any  $n$  the densities are invariant under  $\lambda \rightarrow -\lambda$ , reflecting parity invariance. The qualitative features of the root densities are very similar with varying  $\alpha$ . For  $\lambda \rightarrow 0$ ,  $\eta_n(\lambda)$  with even  $n$  always diverges, as shown for  $n = 2$ . For  $\alpha < 1$  the root densities are non-analytic at  $\lambda = 0$ .

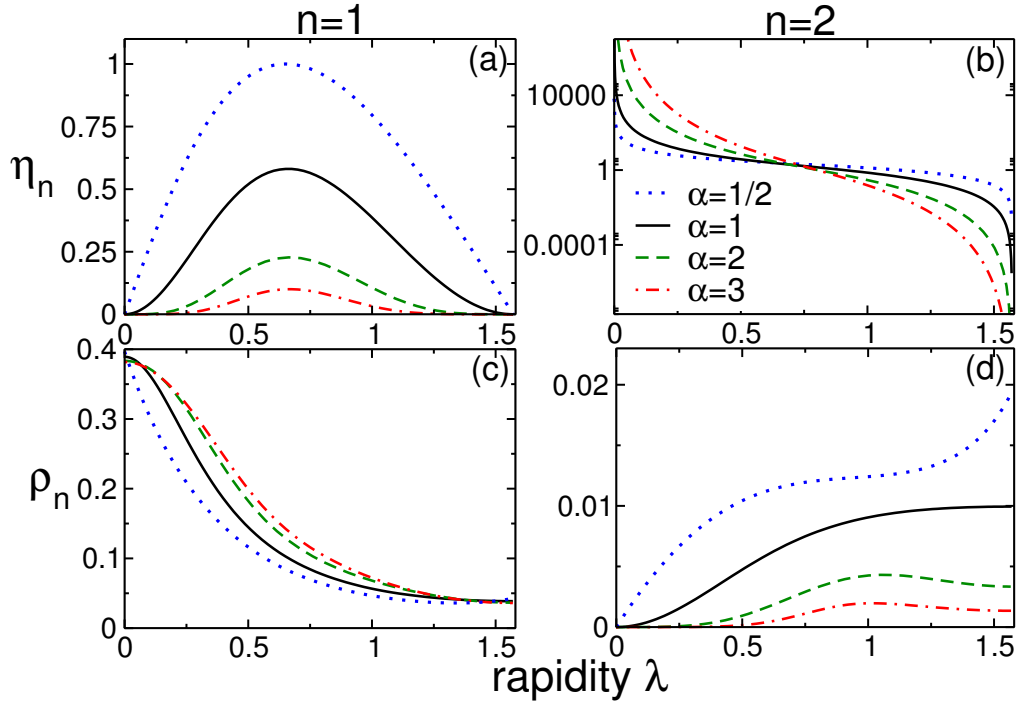


**Figure 1.** Thermodynamic Bethe Ansatz approach for the diagonal Rényi entropies: saddle point rapidity densities  $\rho_n, \eta_n$ . Because of parity invariance only the interval  $[0, \pi/2]$  is plotted. Panels (a) and (b) show  $\eta_n$  as a function of the rapidity  $\lambda$ , for  $n = 1$  and  $n = 2$ , respectively. Different lines correspond to different Rényi index  $\alpha$ . The data are numerical solutions of (20) and (39) for  $\Delta = 2$ . Panels (c) and (d): The same as in (a) and (b) but for the root density  $\rho_n$ .

We finally report the form of the Rényi diagonal entropies (33) written explicitly in terms of the root distributions as

$$S_d^{(\alpha)} = \frac{L}{1-\alpha} \sum_n \int_0^{\pi/2} d\lambda (-\alpha \epsilon_n + s_n), \quad (46)$$

where

$$\epsilon_n \equiv \rho_n (g_n + 4n \ln 2), \quad (47)$$

$$s_n \equiv \rho_n^{(t)} \ln \rho_n^{(t)} - \rho_n \ln \rho_n - \rho_n^{(h)} \ln \rho_n^{(h)}. \quad (48)$$

Here  $\epsilon_n(\lambda)$  and  $s_n(\lambda)$  are the contributions of the bound states with rapidity  $\lambda$  to the Yang-Yang entropy (26) and to the driving  $\mathcal{E}$  (34), respectively. In (47),  $g_n$  is as defined in (35), while  $\rho_n, \rho_n^{(h)}$  are the saddle point densities obtained by solving (39) and (20).

#### 4. Some analytic results

There are few limiting cases in which the Rényi entropies can be calculated analytically or can be analytically related to some known results. It is very instructive to study in details these limits because they will serve as reference points to check the correctness and accuracy of the numerical solutions for the general case and also to give important

physical insights about the physics of the stationary Rényi entropies. Explicitly we consider the limit of large  $\Delta$  for arbitrary  $\alpha$  and the limits for  $\alpha = 0, 1, \infty$  for arbitrary  $\Delta$ .

#### 4.1. Large $\Delta$ expansion

The expansion for large  $\Delta$  in the case of a quench from the Néel state is non-generic because in the limit  $\Delta \rightarrow \infty$  the Néel state becomes the ground-state of the model and there is no quench. Consequently, increasing  $\Delta$  all observables approach the ground-state values and in particular the entropies become all zero.

The expansion for large  $\Delta$  is conveniently parametrised in powers of

$$z \equiv e^{-\eta}, \quad \text{with} \quad \eta \equiv \text{arcosh}(\Delta). \quad (49)$$

As done in Ref. [91] for  $\alpha = 1$ , we use the ansatz for  $\eta_n$

$$\eta_n(\lambda) = z^{\beta_n} \eta_n^{(0)}(\lambda) \exp[\Phi_n(z, \lambda)], \quad (50)$$

where  $\beta_n$ ,  $\eta_n^{(0)}$  and  $\Phi_n(z, \lambda)$  have to be determined and they all depend on  $\alpha$ . Plugging this ansatz in (39), and using the small  $z$  expansion of the driving term  $g_n(\lambda)$  and of  $a_{nm}$  (see (35) and (21), respectively), the leading order in  $z$  fixes the exponent  $\beta_n$  in (50) as

$$\beta_n = \begin{cases} 0 & n \text{ even}, \\ 2\alpha & n \text{ odd}. \end{cases} \quad (51)$$

Moreover, one finds

$$\eta_n^{(0)}(\lambda) = \begin{cases} |\tan(\lambda)|^{-2\alpha} & n \text{ even}, \\ c_n |\sin(2\lambda)|^{2\alpha} & n \text{ odd}, \end{cases} \quad (52)$$

where the constants  $c_n$  are defined as

$$c_n \equiv 4^\alpha \exp \left[ \frac{1}{\pi(1 + \delta_{n,1})} \int_{-\frac{\pi}{2}}^{\frac{\pi}{2}} \ln(1 + |\tan(\lambda)|^{-2\alpha}) \right]. \quad (53)$$

Furthermore  $\Phi_n(0, \lambda) = 0$  so that the small  $z$  behaviour is entirely encoded in  $\beta_n$  and  $\eta_n^{(0)}$ . These results are valid for arbitrary values of  $\alpha$ . Eq. (52) in particular implies that  $\eta_n(\lambda)$  diverges in the limit  $\lambda \rightarrow 0$  for even  $n$ , whereas it is vanishing for odd  $n$ . We numerically observed in the previous section that this feature is generic for any finite  $\Delta$ . The behaviour at the origin is determined by the Rényi index  $\alpha$ .

It is straightforward to show that at this leading order in  $z$ , the Rényi entropies are vanishing. Indeed using Eq. (44), we have  $\rho_1(\lambda) = 1/(2\pi)$ ,  $\rho_{n>1} = \rho_n^{(h)} = 0$ , which leads to  $\mathcal{E}(\rho^*) = S_{YY}(\rho^*) = 0$ . This result reflects the fact that for  $\Delta \rightarrow \infty$  the Néel state is the ground-state of the XXZ Hamiltonian with zero entropy. In order to get a non-zero result, we should perform the expansion up to the first non-zero order. This is easily done for fixed  $\alpha$  (as we will soon do for  $\alpha = 2$ ), but it is more cumbersome to analyse generically having  $\alpha$  as an arbitrary real parameter. It is anyhow easy to understand

the leading term in  $z$  (and hence in  $\Delta$ ). In fact, for arbitrary  $\alpha$ , Eq. (44) joined with (50) provides

$$\rho_1(\lambda) = \frac{1}{2\pi}(1 + 4z \cos(2\lambda) + O(z^2)), \quad \rho_{n>1} = O(z^{2\alpha}), \quad \rho_n^{(h)} = O(z^{2\alpha}). \quad (54)$$

where many of the terms  $O(z^{2\alpha})$  are indeed  $o(z^{2\alpha})$ . Notice that at this order there is no  $\alpha$  dependence. Given that up to  $O(z)$ ,  $\rho_n = \rho_n^{(t)}$ , the corresponding Yang-Yang entropy is vanishing. Thus the Rényi entropies can potentially get a contribution only from the driving term  $\mathcal{E}$ . However, plugging  $\rho_1(\lambda)$  above in (47), we get  $\mathcal{E} = 0$  and so the Rényi entropies are still all vanishing. For  $\alpha > 1$ , the second order (which is  $\alpha$  dependent) gives generically a non-zero result. Again, given that  $\alpha > 1$ , we can ignore the contributions from  $\rho_{n>1}$  and from  $\rho_n^{(h)}$  which are  $O(z^{2\alpha})$ . This again implies that there is no contribution from the Yang-Yang entropy, but that only the second order of  $\rho_1(\lambda)$  provides a non-zero contribution from the driving term  $\mathcal{E}$  which is  $O(z^2)$ . Thus we generically have that for  $\alpha > 1$ , the Rényi entropies are always  $O(z^2)$  as we explicitly show for  $\alpha = 2$  in the following. For  $\alpha = 1$ , the result has been worked out in [91] and we know  $S_{YY} = 4\mathcal{E} = O(z^2)$ , which is compatible with what derived above. Conversely for  $\alpha < 1$ , the terms  $z^{2\alpha}$ , present in many root and hole densities, matter and the analysis becomes more cumbersome. It turns out that the contributions from the driving term and from the Yang-Yang entropy are of the same order, as confirmed also by numerical solutions.

Calculating the expansion of  $\Phi_n(z, \lambda)$  in (50) as power series in  $z$  is easily done for integer  $\alpha$  (while it is slightly more cumbersome for real  $\alpha$ ). Specifically, at a fixed order in the expansion of the TBA system (39) (or (41)) one obtains a finite hierarchy of equations involving only a finite number of the functions  $\Phi_n(z, \lambda)$ . For simplicity in what follows we exhibit explicit formulas only for  $\alpha = 2$ . Up to the fourth order in  $z$ ,  $\Phi_n$  turn out to be

$$\Phi_1 = 4z \cos(2\lambda) + 4z^2(-2 + \sqrt{2})(1 - \cos(4\lambda)) + z^3\left(\frac{4}{3}\cos(6\lambda) - 12\cos(2\lambda)\right) \quad (55)$$

$$- z^4(24(2\sqrt{2} - 3)\cos(4\lambda) - 4(3\sqrt{2} - 4)(3 + \cos(8\lambda))) + \mathcal{O}(z^5),$$

$$\Phi_2 = -16z^2 \cos(2\lambda) + 4z^4(\cos(3\lambda)\sec(\lambda) + \sin(3\lambda)\csc(\lambda)) + \mathcal{O}(z^5), \quad (56)$$

$$\Phi_3 = 8z \cos(2\lambda) + 8z^2(\sqrt{2} - 2)(1 - \cos(4\lambda)) - z^3\left(24\cos(2\lambda) - \frac{8}{3}\cos(6\lambda)\right) \quad (57)$$

$$- z^4(8(12\sqrt{2} - 17)\cos(4\lambda) - 8(3\sqrt{2} - 4)(3 + \cos(8\lambda))) + \mathcal{O}(z^5),$$

$$\Phi_{2k} = \Phi_2, \quad (58)$$

$$\Phi_{2k+1} = \Phi_3. \quad (59)$$

The densities  $\rho_n$  are obtained by plugging the expansion for  $\eta_n(\lambda)$  into (20) (equivalently in (44)). After a straightforward but tedious calculation, we get

$$\begin{aligned} \rho_1 = & \frac{1}{2\pi}(1 + 4z \cos(2\lambda) + 4z^2 \cos(4\lambda) - 8z^3 \sin(2\lambda) \sin(4\lambda) + \\ & + \frac{z^4}{64}(c_1(32 \cos(4\lambda) - 21) - 8(c_1 - 32) \cos(8\lambda))) + \mathcal{O}(z^5), \end{aligned} \quad (60)$$

$$\rho_2 = \frac{3c_1 z^4}{32\pi(1 + \cot^4(\lambda))} + \mathcal{O}(z^5), \quad (61)$$

$$\rho_3 = \frac{3c_1 z^4}{128\pi} + \mathcal{O}(z^5), \quad (62)$$

$$\rho_4 = o(z^4), \quad (63)$$

where  $c_1$  is defined in (53) and for  $\alpha = 2$  it reads  $c_1 = 16(2 + \sqrt{2})$ . In contrast with  $\eta_n$  (cf. (55)-(59)), the leading order of  $\rho_n$  with larger  $n$  corresponds to higher orders in  $z$ . In particular, note that  $\rho_1 = \mathcal{O}(1)$ , whereas  $\rho_2 = \mathcal{O}(z^4)$ , in agreement with the general analysis exposed above for arbitrary  $\alpha$ . The hole densities  $\rho_n^{(h)}(\lambda) = \rho_n(\lambda)\eta_n(\lambda)$  and the total ones  $\rho_n^{(t)} = \rho_n(\lambda) + \rho_n^{(h)}(\lambda)$  are straightforwardly obtained.

From these densities we can finally calculate the leading order in  $z$  of the Yang-Yang entropy associated with the macrostate identified by  $\rho_n$  and  $\eta_n$  given by

$$\begin{aligned} \frac{S_{YY}}{L} &= z^4 \frac{c_1}{2\pi} \left( -4 \ln z \int_{-\frac{\pi}{2}}^{\frac{\pi}{2}} d\lambda \sin^4(2\lambda) + \int_{-\frac{\pi}{2}}^{\frac{\pi}{2}} d\lambda \sin^4(2\lambda) (1 - \ln(c_1 \sin^4(2\lambda))) \right) \\ &\quad + \frac{3}{16} \int_{-\frac{\pi}{2}}^{\frac{\pi}{2}} d\lambda \frac{\ln(\cot^4(\lambda) + 1) + \cot^4(\lambda) \ln(\tan^4(\lambda) + 1)}{\cot^4(\lambda) + 1} + o(z^4) \\ &= z^4 c_1 \left( -\frac{3}{4} \ln z - \frac{1}{4} - \frac{3\pi}{32\sqrt{2}} \right) + o(z^4), \end{aligned} \quad (64)$$

which is compatible with the general behaviour  $z^{2\alpha}$ . In Eq. (64) some miraculous cancellations between the terms coming from  $\rho_1$  and  $\rho_2$  happen, signalling that there could be some hidden structure. The leading contribution of the driving term  $\mathcal{E}$  is

$$\begin{aligned} \frac{\mathcal{E}}{L} &= \frac{1}{\pi} \int_0^{\frac{\pi}{2}} d\lambda \left\{ \frac{1}{4} \ln(4 \sin^2(2\lambda)) + z \cos(2\lambda) (1 + \ln 4 + \ln(\sin^2(2\lambda))) \right. \\ &\quad \left. + z^2 \left[ 2 + \cos(4\lambda) (2 + \ln 4 + \ln(\sin^2(2\lambda))) \right] \right\} \\ &= \frac{z^2}{\pi} \int_0^{\frac{\pi}{2}} d\lambda \left[ 2 + 2 \cos(4\lambda) \ln \sin(2\lambda) \right] = \frac{z^2}{2}, \end{aligned} \quad (65)$$

where we used that the first two orders in (65) and some parts in the third order vanish. The leading orders of  $S_{YY}$  and  $\mathcal{E}$  are then given by different powers of  $z$  being  $z^4 \ln z$  and  $z^2$  respectively. Consequently, for large  $\Delta$ ,  $S_{YY}$  is subleading compared with  $\mathcal{E}$ , implying that the Rényi diagonal entropy for  $\alpha = 2$  is dominated by the driving term in the limit  $z \rightarrow 0$ , as we have generically shown to be the case for  $\alpha > 1$ .

A final observation is now in order. The function which is integrated in Eq. (64) to get  $S_{YY}$  is positive for any  $\lambda$ . Conversely, the function integrated for  $\mathcal{E}$  in Eq. (65) is negative for some values of  $\lambda$ . Since the latter dominate the sum, we have that the integrated function cannot be considered as the contribution of the Bethe mode with momentum  $\lambda$  to the entropy, because this must be a positive function.

#### 4.2. The max entropy, i.e. the limit $\alpha \rightarrow 0$

It is instructive to explicitly consider the limit  $\alpha \rightarrow 0$  of Eq. (46) defining the max entropy, which counts the number of eigenstates of the XXZ chain with non-zero Néel

overlap. In this case, the TBA equations (39) become those of the thermal ensemble at infinite temperature (i.e.  $\beta = 0$ , see e.g. [87] for comparison) and so the diagonal entropy is

$$S_d^{(0)} = L \frac{\ln 2}{2}, \quad (67)$$

i.e. half the Yang-Yang entropy of the thermal ensemble at infinite temperature. The factor  $1/2$  in the exponent reflects that only parity-invariant eigenstates can have non-zero Néel overlap. This is in agreement with the well known fact that the total number of eigenstates with non-zero Néel overlap, for large  $L$  scales like  $\propto 2^{L/2}$  [93] (the total number of eigenstates with non-zero overlap with the Néel state has been obtained analytically at  $\Delta = 1$  [93] and at  $\Delta = 0$  [85]).

#### 4.3. The von Neumann entropy, i.e. the limit $\alpha \rightarrow 1$

In [68] it has been shown in full generality that the diagonal entropy at  $\alpha = 1$  is half of the Yang-Yang entropy. It is important to recover this result from the limit  $\alpha \rightarrow 1$  of (46) and (39) to show the self-consistency of our approach. However, we relegate this test to [Appendix A](#) because it does not provide any new physical insight.

#### 4.4. The min entropy, i.e. the limit $\alpha \rightarrow \infty$

We now analyse the min entropy which is obtained by taking the limit  $\alpha \rightarrow \infty$  of the Rényi entropies (5). The same limit for the entanglement Rényi entropies defines the single copy entanglement [103]. Similar to finite  $\alpha$ , the min entropy exhibits volume-law behaviour. Its density is given in terms of a thermodynamic macrostate that here we determine analytically. As clear from the definition of the diagonal min entropy, at a microscopic level this state is the eigenstate with the largest Néel overlap. Interestingly, we observe two different regimes. For large  $\Delta$  the macrostate coincides with the ground state of the XXZ chain. As it is well known, this has zero Yang-Yang entropy and it contains only one-strings (i.e.  $n$ -strings with  $n > 1$  are not present). Oppositely, at low  $\Delta$  the macrostate is an excited state. We find that this has still zero Yang-Yang entropy but it contains non-trivial bound states. The transition between the two behaviours happens at a special value of  $\Delta$  that we determine.

In order to understand the presence of these two regimes, it is instructive to check what happens if one takes the limit  $\alpha \rightarrow \infty$  of the large  $\Delta$  expansion of Sec. 4.1. Because of the term  $(\sin 2\lambda)^{2\alpha}$  in (52) present in  $\eta_n$  for  $n$  odd, one could naively expect  $\eta_n(\lambda) \rightarrow 0$  for  $\alpha \rightarrow \infty$  (unless  $\lambda = \pi/4$ , but this is a measure zero point). But this is not the case, because one should also check that the constants  $c_n$  in (52) stay finite as  $\alpha \rightarrow \infty$ . This is not the case and indeed  $c_n$  can diverge because

$$\int_{-\pi/2}^{\pi/2} \ln(1 + |\tan(\lambda)|^{-2\alpha}) d\lambda = 4\alpha G + o(\alpha), \quad \Rightarrow \quad c_{n>1} \simeq (2ze^{2G/\pi})^{2\alpha}, \quad (68)$$

where  $G = 0.915\dots$  is the Catalan constant. This implies that it is possible to have

$$\lim_{\alpha \rightarrow \infty} \eta_n(\lambda) \rightarrow 0, \quad \forall n \text{ odd.} \quad (69)$$

for any  $\lambda$  only if (assuming that all  $\Phi_n(z, \lambda)$  in (50) do not diverge as  $\alpha \rightarrow \infty$ )

$$\ln(z) \leq -\ln(2) - 2\frac{G}{\pi}. \quad (70)$$

The condition (70) is clearly satisfied for small enough  $z$  (i.e. large enough  $\Delta$ ), but it also suggests that there is a “critical” anisotropy  $\Delta^* \approx 1.93$  above which (69) holds for any  $\lambda$ . We are going to show that this result is qualitatively correct, although, due to the large  $\Delta$  approximation, the value of  $\Delta^*$  from (70) is not accurate.

*4.4.1. The min entropy for  $\Delta > \Delta^*$  and the determination of  $\Delta^*$ .* In order to determine the analytic behaviour of the min entropy for  $\Delta > \Delta^*$  and to self-consistently determine the value of  $\Delta^*$ , the trick is to impose that (69) is satisfied and check that this is indeed possible and that allows us to solve the TBA equations (41). We stress that it would have been very unlikely to get the idea of imposing the condition (69) without having first performed the large  $\Delta$  expansion.

The equations (69) are recursive and couple each  $\eta_n$  with  $\eta_{n\pm 1}$ . Clearly if all the odd  $\eta_n$  are vanishing according to the condition (69), these equations decouple and in the limit  $\alpha \rightarrow \infty$ , they simplify to

$$\ln \eta_n = \begin{cases} \alpha d_2 & n \text{ even,} \\ \alpha d_1 + s \star \ln(1 + e^{\alpha d_2}) & n = 1, \\ \alpha d_1 + 2s \star \ln(1 + e^{\alpha d_2}) & n \text{ odd,} \end{cases} \quad (71)$$

where the functions  $d_n$  are defined in (42). Eq. (71) for  $n$  odd must be intended as a self-consistent equation with the condition (69), i.e. that the rhs should go to  $-\infty$  as  $\alpha \rightarrow \infty$ . In this respect, the fact that  $d_1(\lambda) < 0 \forall \lambda$  for any value of  $\Delta$  pushes this rhs in the right direction and we are only left with the analysis of the convolution integral in (71). The latter can be simplified as follows. Since  $d_2(\lambda) > 0$  for  $\lambda \in [-\pi/4, \pi/4]$  (which is the only relevant integration region in the limit  $\alpha \rightarrow \infty$ ) we can rewrite, as  $\alpha \rightarrow \infty$ , the convolution as

$$s \star \ln(1 + e^{\alpha d_2}) = \alpha s \star d_2(\lambda) \theta(|\lambda| - \pi/4). \quad (72)$$

At this point, in order to be consistent with (69), one requires

$$d_1 + 2s \star d_2 < 0, \quad \text{and} \quad d_1 + s \star d_2 < 0. \quad (73)$$

These inequalities can be analysed using

$$d_n = \sum_{k \in \mathbb{Z}} e^{-2ik\lambda} \frac{\tanh(k\eta)}{k} [(-1)^n - (-1)^k], \quad (74)$$

which leads to

$$\begin{aligned} s \star d_2 = & \frac{1}{4} \sum_{k \in \mathbb{Z}} \left[ e^{-2ik\lambda} \frac{\tanh(k\eta)}{k \cosh(k\eta)} [1 - (-1)^k] + \right. \\ & \left. + \sum_{k \neq k'} e^{-2ik\lambda} \frac{\sin((k - k')\pi/2)}{2\pi(k - k')} \frac{\tanh(k'\eta)}{k' \cosh(k'\eta)} (1 - (-1)^{k'}) \right]. \end{aligned} \quad (75)$$



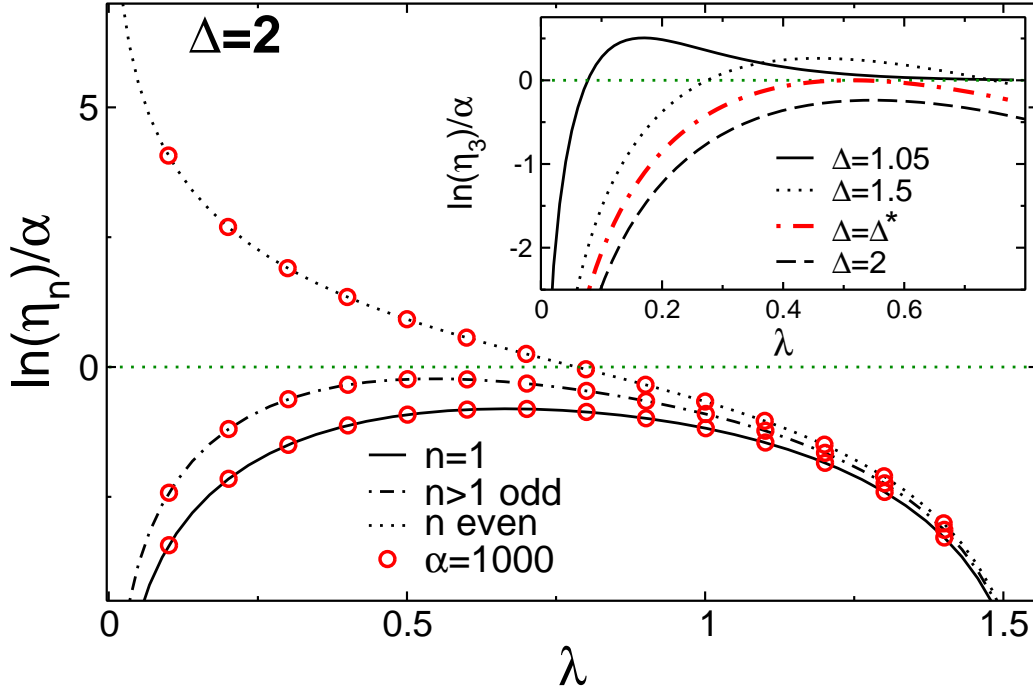


**Figure 2.** Diagonal Rényi entropies in the limit  $\alpha \rightarrow \infty$ : saddle point densities  $\eta_n$  at  $\Delta = 2$ . Main figure:  $\ln(\eta_n)/\alpha$  plotted as a function of the rapidity  $\lambda$ . The lines are the analytical results (71). The circles are obtained by solving numerically the TBA equations for  $\alpha = 10^3$ . For odd  $n$  one has  $\eta_n < 0$  for any  $n$ . Note also that  $\eta_n > \eta_1$  for  $n > 1$ . For even  $n$ ,  $\eta_n$  changes sign at  $\lambda = \pi/4$ , and it diverges at small  $\lambda$ . Inset: The special point  $\Delta^* \approx 1.7669$  at which  $\ln(\eta_n)/\alpha$  (dash-dotted line) touches the real axis.

By using (75) and the expression for  $d_1(\lambda)$  one can work out numerically that (73) holds for  $\Delta > \Delta^* = 1.76692\dots$ , which is slightly lower than the result (70) from the large  $\Delta$  expansion.

The results (71) for  $\eta_n$  are shown in Figure 2. Since  $\eta_n$  are even functions of  $\lambda$ , we restrict ourselves to the region  $\lambda > 0$ . The Figure reports  $\ln(\eta_n)/\alpha$  as functions of  $\lambda$  for  $\Delta = 2$  (plots for other values of  $\Delta > \Delta^*$  are equivalent). The continuous curves correspond to the analytic solution (71) while the circles are obtained by solving numerically the TBA equations for  $\alpha = 10^3$ : the two are in perfect agreement. In particular, one has that  $\ln(\eta_n)/\alpha < 0$  for  $n$  odd, in agreement with (69), while for even  $n$ ,  $\ln(\eta_n)$  is positive for  $|\lambda| < \pi/4$ , and it diverges at  $\lambda \rightarrow 0$ . Note also that for any  $\lambda$  one has  $\eta_3 > \eta_1$  (we recall that all  $\eta_n$  with  $n$  odd and  $n \neq 1$  are equal). The inset in the Figure shows  $\ln(\eta_3)/\alpha$  for various  $\Delta$  both larger and smaller than  $\Delta^* \approx 1.7669$  (cf. (73)). For  $\Delta < \Delta^*$  there is an extended region where  $\ln(\eta_3) > 0$ , implying that the condition (69) is violated and the solution (71) is not valid. For  $\Delta = \Delta^*$ ,  $\eta_3(\lambda)$  is tangent to the horizontal axis. The results for  $\eta_n$  in the region with  $\Delta < \Delta^*$  are discussed in 4.4.2.

We are now ready to derive analytically  $\rho_n$  for  $\Delta \geq \Delta^*$ . Again, it is instructive to look at what happens in the large  $\Delta$  limit (see (60)). As discussed above, we have

$\rho_1 = \mathcal{O}(1)$  and  $\rho_{n>1} \sim \mathcal{O}(z^{2\alpha})$ . Thus in the limit  $\alpha \rightarrow \infty$  we have

$$\rho_n \rightarrow 0, \quad n \geq 2. \quad (76)$$

On the other hand, from (20),  $\rho_1$  is determined by solving the integral equation

$$\rho_1 = a_1 - a_{11} \star \rho_1. \quad (77)$$

To derive (77) we used that  $\rho_1^{(h)} \rightarrow 0$  because  $\eta_1 \rightarrow 0$  (cf. (71)) and  $\rho_1$  is assumed to be regular. Eq. (77) is the same integral equation that identifies the ground state root density of the XXZ chain [87] which is solved by Fourier transform providing

$$\rho_1 = s(\lambda) = \frac{1}{2\pi} \sum_{k \in \mathbb{Z}} \frac{e^{2ik\lambda}}{\cosh(k\eta)}. \quad (78)$$

The energy of the state reads

$$\frac{E}{L} = -\sinh(\eta) \sum_{k \in \mathbb{Z}} \frac{1}{e^{2|k|\eta} + 1}. \quad (79)$$

Eq. (78) and (76) can be also found without relying on the small  $z$  expansion. Indeed, plugging the condition (69) in the recursive equations (44) we have for the even densities  $\rho_{2k}(\lambda)(1 + \eta_{2k}(\lambda)) \rightarrow 0$ , i.e.  $\rho_{2k}(\lambda) \rightarrow 0 \forall k$ . Plugging this result for even  $n$  in (44), we obtain also the odd densities as  $\rho_{2k+1}(\lambda) \rightarrow 0$  for  $k > 0$ , and

$$\rho_1(\lambda) = s(\lambda), \quad (80)$$

which is the same as (78) and correspondst to the ground-state of the XXZ spin-chain.

*4.4.2. The min entropy for  $\Delta < \Delta^*$ .* For  $\Delta < \Delta^*$  it is convenient to use the parametrisation

$$\eta_n = \exp(\alpha\gamma_n). \quad (81)$$

Here the finite functions  $\gamma_n(\lambda)$  have to be determined by solving the TBA system (41) for  $\eta_n$ . In the limit  $\alpha \rightarrow \infty$  the equations for  $\gamma_n$  are obtained from (41) as

$$\gamma_n = d_n + s \star [\gamma_{n-1}^+ + \gamma_{n+1}^+], \quad \gamma_n^+(\lambda) \equiv \begin{cases} \gamma_n(\lambda) & \text{if } \gamma_n(\lambda) > 0, \\ 0 & \text{if } \gamma_n(\lambda) < 0. \end{cases} \quad (82)$$

In the right-hand side only the positive part  $\gamma_n^+$  of  $\gamma_n$  appear, which makes the equations non linear. The values of  $\lambda$  where  $\gamma_n$  change sign have also to be determined from (82).

The fact that  $\eta_n(\lambda)$  either diverges or vanishes in the large  $\alpha$  limit (except in special points when  $\gamma_n = 0$ ) implies that  $\rho_n(\lambda)$  and  $\rho_n^{(h)}(\lambda)$  have complementary domains in which they are non zero (under the reasonable assumption that they are finite, except in isolated points). In particular  $\rho_n(\lambda)$  is non-zero only for those  $\lambda$  such that  $\gamma_n(\lambda) < 0$  and viceversa for  $\rho_n^{(h)}(\lambda)$ . Because of the complementarity of the domains, the TBA equations (20) for  $\rho_n(\lambda)$  and  $\rho_n^{(h)}(\lambda)$  decouple. First the non zero-part of  $\rho_n(\lambda)$  is obtained by solving the equations

$$\rho_n(\lambda) = a_n(\lambda) - \sum_{m=1}^{\infty} (a_{nm} \star \rho_m)(\lambda), \quad (83)$$

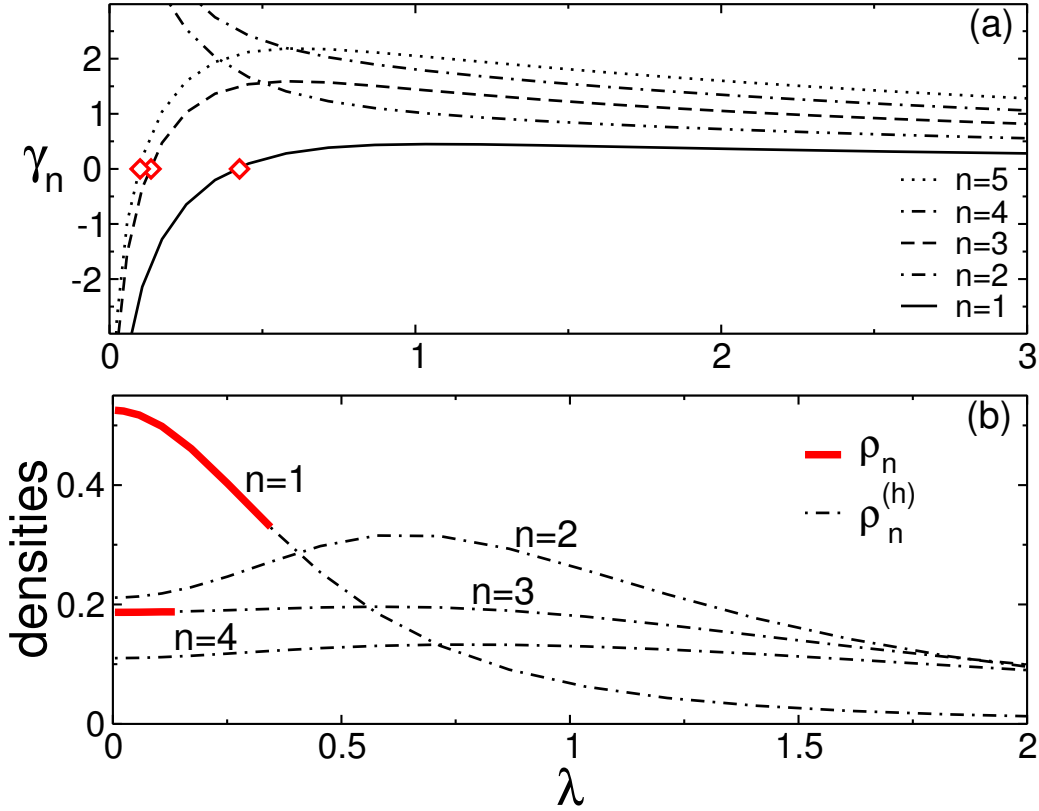


**Figure 3.** Diagonal Rényi entropies in the limit  $\alpha \rightarrow \infty$  in the XXX chain. Panel (a): Saddle point  $\gamma_n \equiv \ln(\eta_n)/\alpha$  as a function of rapidity  $\lambda$ . For even  $n$ ,  $\gamma_n$  are positive and diverge at small  $\lambda$ , while they vanish for  $\lambda \rightarrow \infty$ . For odd  $n$ ,  $\gamma_n \rightarrow -\infty$  at small  $\lambda$ . The diamonds mark the points where  $\gamma_n$  change sign. Panel (b): Particle densities  $\rho_n$  (full lines) and hole densities  $\rho_n^{(h)}$  (dash-dotted lines). Only the non-zero values of  $\rho_n$  and  $\rho_n^{(h)}$  are shown. Note that both densities are not continuous functions.  $\rho_n$  is non-zero only for odd  $n$ . For generic  $n$ ,  $\rho_n$  ( $\rho_n^{(h)}$ ) is non-zero only if  $\gamma_n$  is positive (negative) (see Figure 2).

where each  $\rho_m$  is non zero only where  $\gamma_n(\lambda) < 0$ . Similarly,  $\rho_n^{(h)}$  is non-zero only on the support of  $\gamma_n^+$ . From the solutions  $\rho_n$  of (83)  $\rho_n^{(h)}$  is obtained as

$$\rho_n^{(h)} = a_n - \sum_{m=1}^{\infty} (a_{nm} \star \rho_m), \quad (84)$$

which seems the same as (83), but it is defined in the complementary domain.

Equations (82), (83), and (84) cannot be handled analytically, but are easily solved numerically. Their numerical solutions for  $\gamma_n$  and  $\rho_n$  are reported in Figure 3 for  $\Delta = 1$  (for which  $\lambda$  is defined on the entire real axis). Panel (a) shows  $\gamma_n$  for  $n \leq 5$  as obtained by numerically solving (82). Due to the parity symmetry, we only show results for  $\lambda \geq 0$ . For even  $n$ ,  $\gamma_n$  are positive for any  $\lambda$ , and they diverge as  $\lambda \rightarrow 0$  so that  $\rho_{2k} \rightarrow 0$  in the same limit. On the other hand, for odd  $n$ ,  $\gamma_n \rightarrow -\infty$  at small  $\lambda$ , whereas  $\gamma_n$  is positive for large enough  $\lambda$ . Thus  $\gamma_n$  for odd  $n$  must change sign at least once: the points where this happens are marked with the diamonds in Figure 3 (a).

Numerical results for  $\rho_n$  are reported in Figure 3 (b). The continuous lines are the particle densities  $\rho_n$ , while the dash-dotted lines are the hole densities  $\rho_n^{(h)}$ . For even  $n$ ,  $\rho_n$  is identically zero, as expected, while for odd  $n$  particle and hole densities have complementary support. Thus for any  $n$ ,  $\rho_n^{(t)}(\lambda)$  is either equal to  $\rho_n^{(h)}(\lambda)$  or to  $\rho_n(\lambda)$  and so the thermodynamic macrostate has zero Yang-Yang entropy.

*4.4.3. Results for the min entropy.* Given that in both regimes  $\Delta > \Delta^*$  and  $\Delta < \Delta^*$  the Yang-Yang entropy of the macroscopic state is zero, the min entropy is just given by the overlap (driving) term (47) as

$$S_d^{(\infty)} = L \sum_n \int_0^{\pi/2} d\lambda \rho_n(\lambda) (g_n(\lambda) + 4n \ln 2), \quad (85)$$

with  $g_n$  defined in (35). Thus, as it should, the min entropy identifies a single eigenstate with the largest overlap that for  $\Delta > \Delta^*$  is the ground-state. The  $\Delta$  dependence of the min entropy is reported in Figure 4 (together with the results for other values of  $\alpha$ ). At  $\Delta = \Delta^*$  there is a transition between two curves which anyhow is very smooth. The inset of the Figure compares for  $\Delta < \Delta^*$  the logarithm of the overlap of the ground-state (i.e. the analytic continuation of the curve for  $\Delta > \Delta^*$ ) with the actual min entropy, showing that the difference is sizeable only for  $\Delta$  very close to 1.

The energy of the state with the largest overlap is shown in Figure 5 (again together with the results for other values of  $\alpha$ ). For  $\Delta \geq \Delta^*$ , this is the energy of the ground state of the XXZ chain (shown as dash-dotted line in the Figure). The small circles for  $\Delta < \Delta^*$  are the results obtained using the saddle point densities in 4.4.2 and again the transition between the two regimes is very smooth. The largest difference is at  $\Delta = 1$  for which  $E/L \approx -0.66$  compared to the ground state energy density  $-\ln 2 \approx -0.693$ .

## 5. General results for the Rényi entropies

In this section we report the results for the diagonal Rényi entropies  $S_d^{(\alpha)}$  which are half of the thermodynamic ones. Figure 4 shows numerical results obtained from Eq. (46) in which we plugged the solution for the root densities of the TBA equations (39) (or equivalently (41)) for the quench from the Néel state. The entropy densities  $S_d^{(\alpha)}/L$  are plotted as a function of the chain anisotropy  $\Delta$ . All the entropies are vanishing in the limit  $\Delta \rightarrow \infty$ , because the Néel state is the ground state of the XXZ chain in that limit and in agreement with the result of the previous section. For  $\alpha = 1$  the data correspond to  $S_{YY}/2$  which is obtained by using the analytical results for the thermodynamic macrostate in Ref. [91]. From the Figure it is clear that  $S_d^{(\alpha)} \leq S_d^{(\alpha')}$  for  $\alpha' < \alpha$ , as expected. For  $\alpha = \infty$ , the dash-dotted line is the result for  $\Delta > \Delta^*$  (obtained in section 4.4.1), whereas the small circles are for  $\Delta \leq \Delta^*$  (see 4.4.2). The value of  $\Delta^* \approx 1.7669$  is marked by the triangle.

A last consistency check is provided by the general inequality

$$S_d^{(2)} = -\ln \sum_n w_n^2 \leq -2 \ln(\max_n w_n) = 2S_d^{(\infty)}, \quad (86)$$

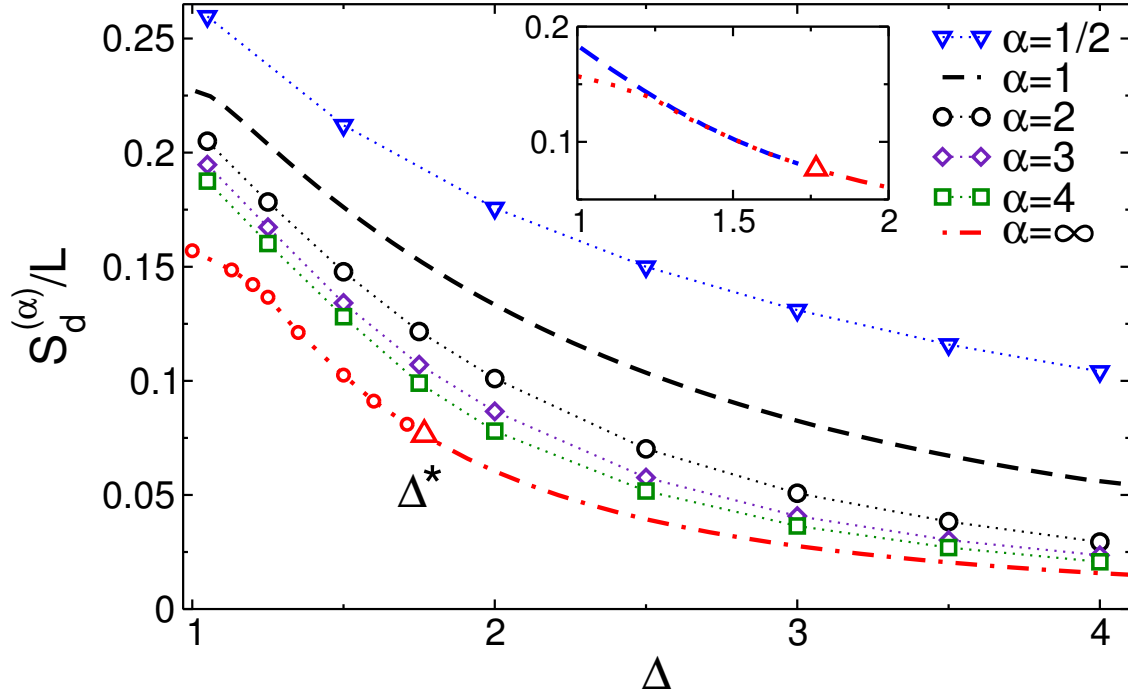


**Figure 4.** Thermodynamic Bethe Ansatz results for the Diagonal Rényi entropy density  $S_d^{(\alpha)}/L$  after the quench from the Néel state in the XXZ chain as a function of the anisotropy  $\Delta$ . The dashed line is the von Neumann entropy for  $\alpha = 1$ . Different symbols are used for different  $\alpha$ . The result for  $\alpha \rightarrow \infty$  is also shown (the triangle marks the special point  $\Delta^*$ ). Inset:  $S_d^{(\infty)}/L$  for  $\Delta < \Delta^*$ . The dotted line is the result in the main Figure. The dashed line is obtained using the same saddle point densities as for  $\Delta > \Delta^*$ .

which is satisfied by all our data. From the TBA point of view, this is a non trivial check because it is based on the solution of different TBA equations. We numerically observe that (86) is saturated for large  $\Delta$  because the sums in (86) are dominated by the largest overlap, which is separated by a gap from the smaller overlaps.

### 5.1. Energy of the macrostate

It is an interesting exercise to investigate the energy density of the macrostate  $\rho_n$  because it depends on  $\alpha$ , implying that it is different from that describing the stationary behaviour of local observables. The latter is recovered in the limit  $\alpha = 1$ . The energy of the macrostate provides information about the region in the energy spectrum of the XXZ model that is relevant to describe the Rényi diagonal entropies. We have already seen that  $\alpha = 0$  is equivalent to the infinite temperature state, while  $\alpha \rightarrow \infty$  approaches the ground state of the model (at least for  $\Delta > \Delta^*$ ), i.e. zero temperature. Hence, by varying  $\alpha$  we explore the entire energy window relevant for the XXZ spin-chain.

Our results are shown in Figure 5, reporting the energy density  $E/L$  of the macrostate as a function of  $\Delta$ . This is readily obtained plugging the densities  $\rho_n$  (cf. (20) and (39)) in (25). The symbols are results for different values of  $1/2 \leq \alpha \leq \infty$ . The

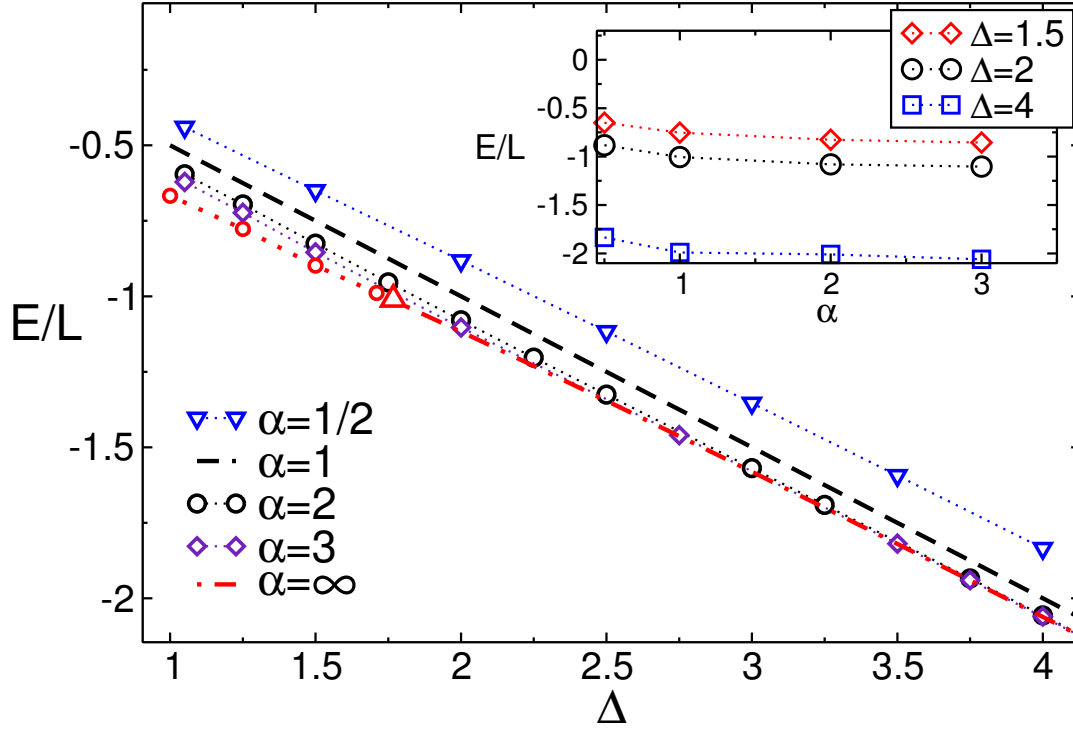


**Figure 5.** Energy density  $E/L$  of the saddle point representative state for the diagonal Rényi entropies plotted versus the chain anisotropy  $\Delta$  for several values of the Rényi index  $\alpha$ . The dashed line is the exact result  $E/L = -\Delta/2$  for  $\alpha = 1$ . On the line  $\alpha \rightarrow \infty$  the triangle marks the special point  $\Delta^*$ . The inset shows the  $\alpha$  dependence of  $E/L$  for three values of  $\Delta$ .

dashed line is for  $\alpha = 1$ , which corresponds to  $E/L = \langle \Psi_0 | H | \Psi_0 \rangle = -\Delta/2$ . For all values of  $\alpha$ , the large  $\Delta$  behaviour is straightforwardly calculated plugging (54) into (15) obtaining

$$\frac{E}{L} = -\frac{\Delta}{2} - \frac{1}{4\Delta} + O(\Delta^{-2}), \quad (87)$$

independently from  $\alpha$ . Higher orders in  $\Delta$  do depend on  $\alpha$ . The explicit  $\alpha$  dependence is reported in the inset for fixed value of  $\Delta$ . From this inset, it is clear that the various curves are very similar and the main difference is the shift in energy.

## 5.2. Numerical checks

In this section we provide numerical evidence for the results presented in section 3. We employ two different methods: in subsection 5.2.1 by using exact (full) diagonalisation techniques we construct explicitly the diagonal ensemble (4) and the diagonal Rényi entropies (cf. (5)) for chains of length  $L \leq 22$ ; in subsection 5.2.2 the diagonal Rényi entropies are obtained numerically by exploiting the knowledge of the overlaps between the Néel state and the Bethe eigenstates, following the approach of Ref. [93].

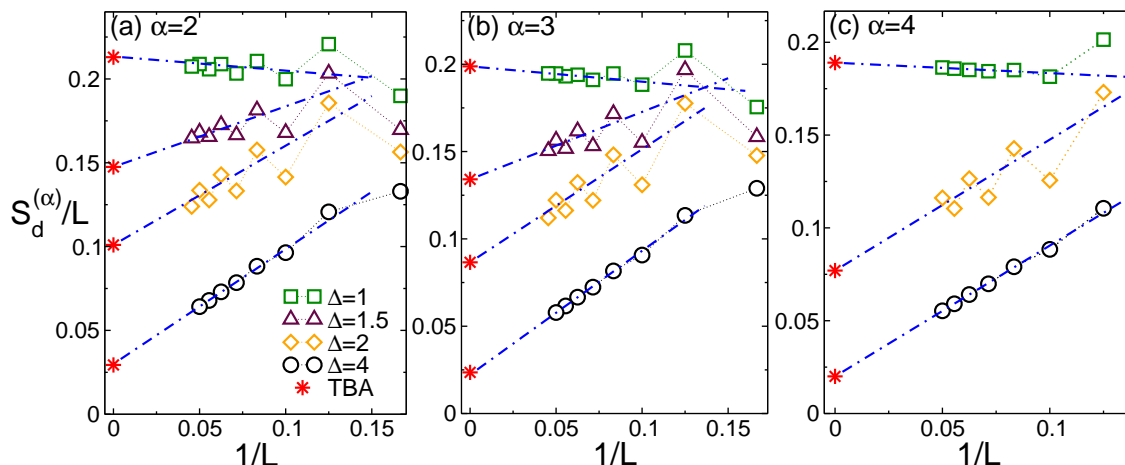


**Figure 6.** Diagonal Rényi entropies after the quench from the Néel state for several values of  $\Delta$ :  $S_d^{(\alpha)}/L$  plotted against the inverse chain length  $1/L$ . Panels (a), (b) and (c) correspond to  $\alpha = 2$ ,  $\alpha = 3$ , and  $\alpha = 4$  respectively. The stars are the TBA results in the thermodynamic limit. The dash-dotted lines are fits to  $S_d^{(\alpha)}/L = s_\infty^{(\alpha)} + b_\alpha/L$ , with  $s_\infty^{(\alpha)}$  fixed to the Bethe ansatz result, and  $b_\alpha$  fitting parameters.

*5.2.1. Exact diagonalisation.* The symmetric Néel state (9) has zero magnetisation, and it is invariant under both one-site translations and under parity inversion. Thus, only eigenstates in the sector with zero magnetisation, zero momentum, and invariant under parity can have non zero Néel overlap (see Ref. [104] for the implementation of these symmetries in exact diagonalisation). Here we restrict ourselves to this sector of the Hilbert spaces. For  $L = 22$  this contains  $N = 16159$  eigenstates. This is a small fraction of the total number of eigenstates  $2^{22} \sim 4 \cdot 10^6$  of the XXZ chain, although it is still quite large compared with the number of parity-invariant eigenstates (i.e. the only ones with non-zero Néel overlap), which is  $\sim 2^{L/2-1} \sim 500$  [85, 93]. In section 5.2.2 by exploiting this property within the formalism of Bethe ansatz, we will construct the diagonal ensemble for chains with  $L \approx 40$ .

Our exact diagonalisation results are discussed in Figure 6, showing  $S_d^{(\alpha)}$  for  $\alpha = 2$ ,  $\alpha = 3$ ,  $\alpha = 4$  (panel (a), (b), and (c) respectively) plotted versus  $1/L$ . Finite-size effects are visible for all values of  $\alpha$ . Interestingly, in the region  $\Delta \approx 1$  these oscillate with the parity of  $L/2$ . The star symbols denote the diagonal entropy densities  $s_\infty^{(\alpha)}$  in the thermodynamic limit, which are obtained using (33). The dash-dotted lines are linear fits to  $S_d^{(\alpha)} = s_\infty^{(\alpha)} + a_\alpha/L$ , with  $s_\infty^{(\alpha)}$  fixed by (33). The agreement between the data and (33) is satisfactory for  $\Delta = 1$  and at large  $\Delta$ . For intermediate values of  $\Delta$  the large oscillations do not allow for a reliable confirmation of the theoretical results, although the data are clearly compatible with (33).

*5.2.2. Numerical Bethe ansatz,* We now provide a further check of (33) by constructing the diagonal Rényi entropies using the exact overlaps between the eigenstates of the XXZ model and the Néel state. These can be calculated from the solutions of the Bethe-

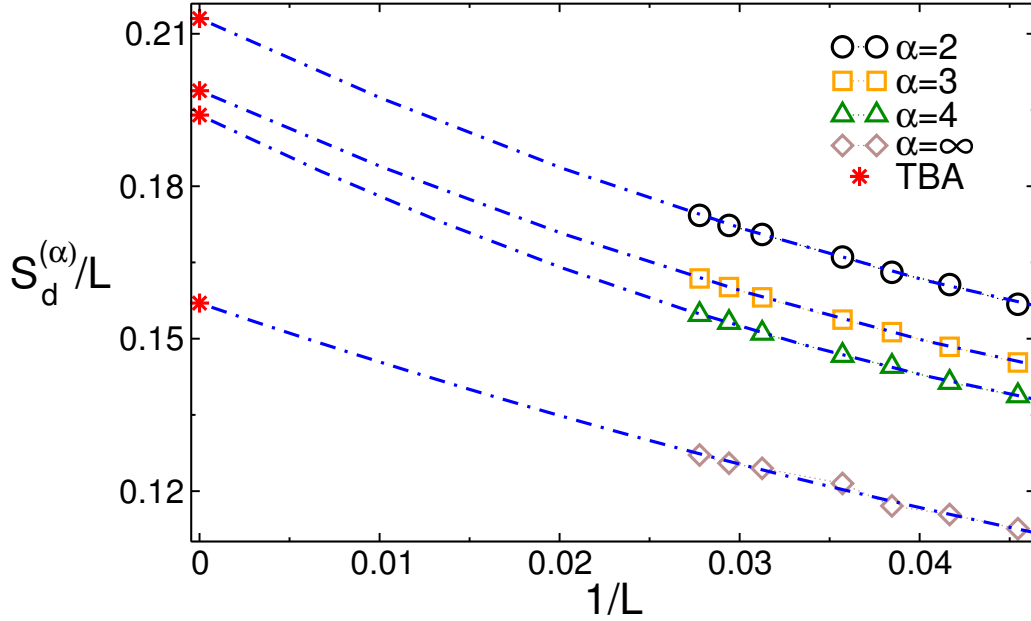


**Figure 7.** The Rényi diagonal entropies in the  $XXZ$  chain after the Néel quench. The data are obtained by using the exact overlaps between the Bethe eigenstates and the Néel state. The entropies density  $S_d^{(\alpha)}/L$  is plotted against the inverse chain length  $1/L$  for several values of  $\alpha$ . The star symbols are the Bethe ansatz results in the thermodynamic limit. The dash-dotted lines are fits to  $S_d^{(\alpha)} = s_\infty^{(\alpha)} + a_\alpha/L + b_\alpha/L^2$ , with  $s_\infty^{(\alpha)}$  fixed to the TBA result and  $a_\alpha, b_\alpha$  fitting parameters.

Gaudin-Takahashi equations (13) using the Algebraic Bethe Ansatz [78,80,91]. Although this is possible, in principle, for all the  $XXZ$  chain eigenstates, a technical problem arises for eigenstates that correspond to solutions of the BGT equations containing zero momentum strings, i.e., with vanishing string center. Precisely, some fictitious singularities appear in the overlap formulas, which have to be removed. To overcome this issue one needs to go beyond the string hypothesis, considering the finite-size behaviour of the string deviations (12). This is a formidable task that in practice can be performed only for small chains. It has been shown that in the thermodynamic limit the vast majority of eigenstates of the  $XXZ$  chain with finite Néel overlap contain zero-momentum strings. More precisely, the ratio between the total number of parity-invariant eigenstates  $Z_{Neel}$  and the ones without zero-momentum strings  $\tilde{Z}_{Neel}$  vanishes in the thermodynamic limit as [93]

$$\frac{\tilde{Z}_{Neel}}{Z_{Neel}} \propto \frac{4}{\sqrt{\pi L}}. \quad (88)$$

As a consequence of (88), all the expectation values calculated on the restricted ensemble constructed by excluding the zero-momentum strings vanish in the thermodynamic limit. For instance, one has

$$w_{\Psi_0} \equiv \sum_m^I |\langle m | \Psi_0 \rangle|^2 \rightarrow 0, \quad (89)$$



where the prime is to stress that only eigenstates that do not contain zero-momentum strings are included in the sum. On the other hand, for any finite size and any normalised initial state  $|\Psi_0\rangle$  it should be  $\sum_m |\langle m|\Psi_0\rangle|^2 = 1$ . However, it has been suggested in Ref. [91] and confirmed numerically in [93] that eigenstates containing zero-momentum strings are irrelevant in the thermodynamic limit. The idea proposed in [93] is that the diagonal ensemble expectation values must be renormalised by the factor  $w_{\Psi_0}$  in (89). The diagonal Rényi entropies in this approach are given by

$$S_d^{(\alpha)} = \frac{1}{1-\alpha} \ln \left[ \frac{1}{w_{\Psi_0}^\alpha} \sum_m' |\langle m|\Psi_0\rangle|^{2\alpha} \right]. \quad (90)$$

This reweighted expression converges for large  $L$  to the thermodynamic expectation value, but has different  $1/L$  finite-size corrections [93].

In Figure 7 we report the numerical results from (33) for the Néel quench at  $\Delta = 1$ . The symbols correspond to different values of  $\alpha$  ranging from  $\alpha = 2$  to  $\alpha = \infty$ . In the Figure we plot  $S^{(\alpha)}/L$  versus  $1/L$  for chains with  $L \leq 38$ . The star symbols are the theoretical results obtained using the *TBA* approach (cf. (33)). The dash-dotted lines are fits to  $S_d^{(\alpha)}/L = s_\infty^{(\alpha)} + a_\alpha/L + b_\alpha/L^2$ , with  $a_\alpha, b_\alpha$  fitting parameters and  $s_\infty^{(\alpha)}$  the entropy density obtained from Bethe ansatz. The numerical results are clearly compatible with (33) in the thermodynamic limit.

## 6. Entanglement versus diagonal entropies

In this section we discuss the stationary value of the Rényi entanglement entropies of a block  $A$  of  $\ell$  contiguous spins after the Néel quench in the XXZ chain. As stressed in the introduction, the stationary value of the entanglement entropy is equal to the thermodynamic entropy (i.e. the entropy of the GGE) which is the double of the diagonal entropy [68]. This equivalence has been investigated in several studies for the von Neumann entropy, both for free systems [60, 61, 63, 65] and for interacting ones [62, 66–68], but not for the Rényi entropies with  $\alpha \neq 1$ . Here we then perform extensive tDMRG simulations [105–109], to provide numerical evidences that in the limit of large chains and large subsystems, i.e.,  $L, \ell \rightarrow \infty$  with  $\ell \ll L$ , one has

$$\frac{2S_d^{(\alpha)}}{L} = \frac{S_{\text{GGE}}^{(\alpha)}}{L} = \frac{S_A^{(\alpha)}}{\ell}. \quad (91)$$

Before presenting our results for the Rényi entropies, it is worth to recall some generic features about the time evolution of the entanglement entropy after a quench. In many numerical and analytic calculations [23, 71, 110–123], as well as in one experiment [10], it has been observed that the entanglement entropy first grows linearly in time up to a time  $t^*$  proportional to the length of the subsystem and subsequently slowly saturates to the extensive value of the thermodynamic ensemble. For an integrable model, this behaviour can be explained in terms of a quasi-particle picture introduced in [71]. According to this picture, the prequench initial state acts as a source of pairs of quasiparticle excitations with velocity  $v(\lambda)$ . Although quasiparticles created far apart

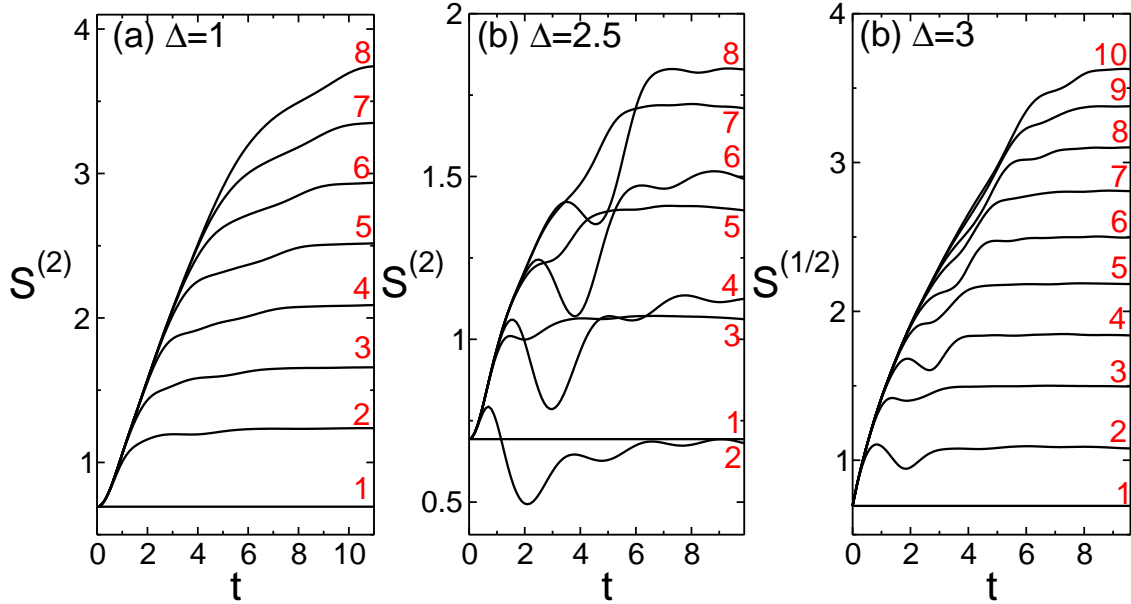


**Figure 8.** Rényi entanglement entropies after the quench from the Néel state in the XXZ chain: tDMRG results for  $L = 40$  plotted as a function of time. Different curves correspond to different subsystem sizes (accompanying numbers). Panels (a) and (b) show data for  $S^{(2)}$  at  $\Delta = 1$  and  $\Delta = 2.5$ , respectively. Panel (c) shows data for  $S^{(1/2)}$  for  $\Delta = 3$ . Note at short time the sizable oscillations for  $\ell$  even.

from each other are incoherent, those emitted at the same point in space are entangled. Because these propagate ballistically throughout the system, larger regions get entangled while time passes. At time  $t$ , the entanglement entropy is proportional to the total number of quasiparticle pairs that, emitted at the same point in space, are shared between A and its complement. When a maximum quasiparticle velocity  $v_M$  exists, then for  $t \leq \ell/(2v_M) = t^*$  the entropy increases linearly. This picture has been used in [56] to provide a prediction for the entanglement entropy which becomes exact in the space-time scaling limit (i.e. for  $t, \ell \rightarrow \infty$  with  $t/\ell$  fixed). Conversely, for non-integrable models, quasiparticles have usually a finite life-time and the picture above could be used only to have some gross features for the time evolution of the entanglement entropy. However, the linear increase of the entanglement followed by saturation has been observed generically for non-integrable models and its origin is likely to have also an alternative explanation, see e.g. [123, 124].

An overview of our tDMRG data for the entanglement entropy  $S_A^{(\alpha)}$  is reported in Figure 8. The data are for  $\alpha = 2$  (panel (a) and (b)) and  $\alpha = 1/2$  (panel (c)). In each panel, the different curves correspond to different subsystem sizes  $\ell \lesssim 10$ . The data are obtained by Trotter evolution of the Matrix Product State representation of the Néel state. The largest bond dimension employed in the simulation is  $\chi = 400$ . The Trotter time discretisation step is  $\delta t = 0.05$ . For  $\Delta = 1$ ,  $S^{(2)}$  exhibits a quite linear smooth increase with time and a saturation at  $t \propto \ell$ , as it should. At larger  $\Delta$ , sizable odd-even effects are present (see (b) in the Figure) and the data for even  $\ell$  show large oscillating

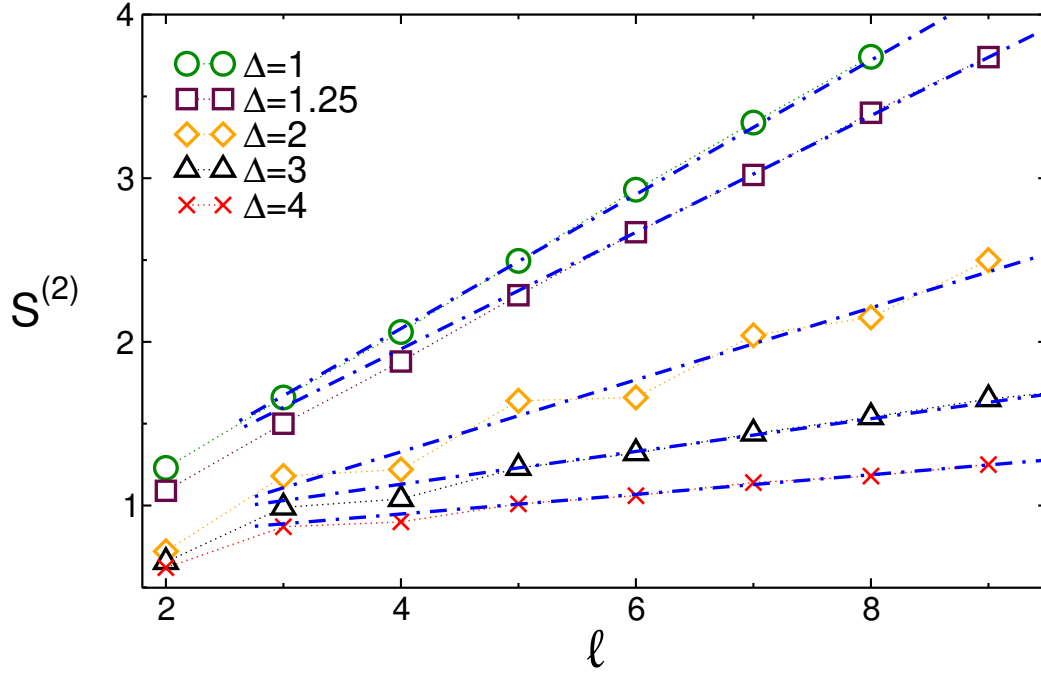


**Figure 9.** Stationary Rényi entanglement entropy  $S^{(2)}$  in the XXZ chain for different values of  $\Delta$  as function the subsystem length  $\ell$ . The points are tDMRG results for a chain with  $L = 40$  at  $t \sim 10$ . The dash-dotted lines are fits to  $S^{(2)} = s_{\infty}^{(2)}\ell + a_2$ , with  $a_2$  a fitting parameter and  $s_{\infty}^{(2)}$  fixed to the density of the GGE Rényi entropy obtained from the Bethe ansatz.

corrections with time. This is likely to be imputed to the relative small value of  $\ell$  accessible by tDMRG and these oscillations are expected to disappear in the space-time scaling limit. A similar, but less pronounced, behaviour is observed for  $\alpha = 1/2$  ((c) in the Figure).

In Figure 9 we focus on the steady-state value of  $S^{(2)}$ . The symbols denote the stationary values of  $S^{(2)}$  (tDMRG data at  $t \approx 10$ , see Figure 8) for different values of  $\Delta$  plotted against the subsystem length  $\ell$ . The expected volume law  $S^{(2)} \propto \ell$  is clearly visible. Moreover,  $S^{(2)}$  decreases monotonically with increasing  $\Delta$ , similar to the von Neumann entropy [56]. This reflects that for  $\Delta \rightarrow \infty$  the Néel state becomes the ground state of the XXZ chain. The dash-dotted lines are linear fits to

$$S^{(\alpha)} = a_{\alpha} + s_{\infty}^{(\alpha)}\ell, \quad (92)$$

with  $\alpha = 2$ ,  $a_2$  a fitting parameter and  $s_{\infty}^{(2)}$  the density of the GGE Rényi entropy, as obtained from Bethe ansatz (33). The agreement with the numerical data is perfect already for  $\ell \gtrsim 5$  (although there are oscillations with the parity of  $\ell$  for  $\Delta = 2$ ). This allows us to conclude that, within the system sizes accessible with DMRG, the numerical data confirm the validity of (91). In Figure 10 we also consider other values of  $\alpha$ , namely  $\alpha = 1/2$  (circles) and  $\alpha = \infty$  (diamonds) (also old data [56] for  $\alpha = 1$  (squares) are shown for comparison). We restrict ourselves to the relatively large values of  $\Delta = 3, 4$ , for which longer times and larges subsystem sizes can be accessed with

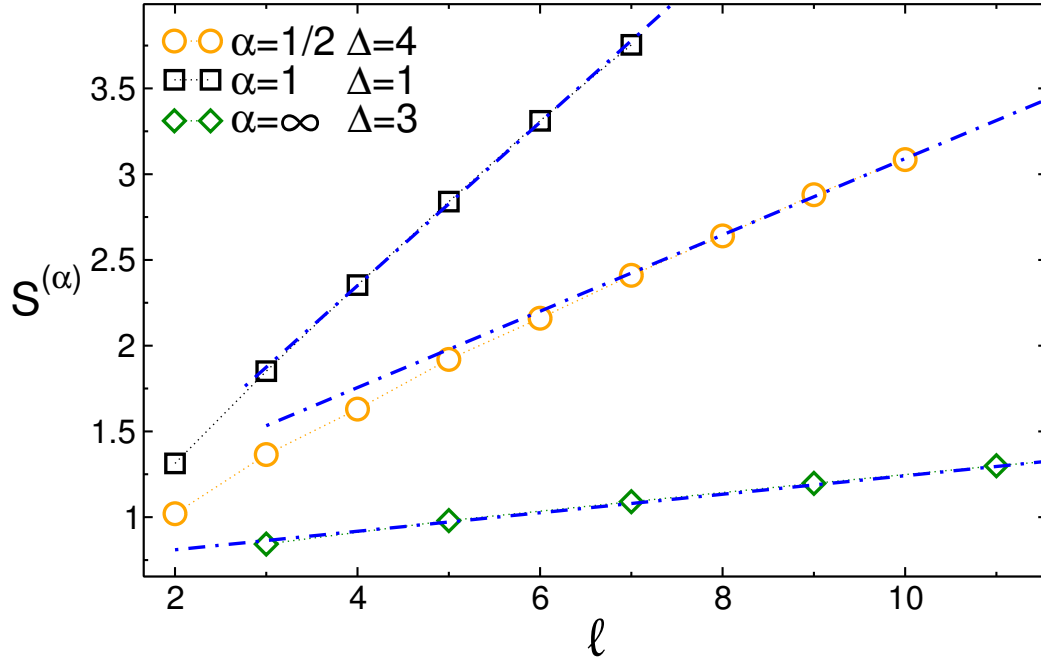


**Figure 10.** Stationary Rényi entanglement entropies after the Néel quench in the XXZ chain for  $\alpha = 1/2, 1, \infty$ . The dash-dotted lines are linear fits to  $S^{(\alpha)} = s_{\infty}^{(\alpha)} \ell + a_{\alpha}$ , with  $s_{\infty}^{(\alpha)}$  the Bethe ansatz density of the GGE Rényi entropies and  $a_{\alpha}$  a fitting parameter.

tDMRG, because of the mild entanglement increase after the quench. For  $\alpha = \infty$  we only show data for odd  $\ell$  because for even  $\ell$  severe finite-size corrections do not allow us to reliably extract the stationary value. Irrespective of  $\alpha$ , the entropies exhibit the expected volume-law behaviour at large  $\ell$ . The dash-dotted lines are fits to (92), with  $a_{\alpha}$  a fitting parameter and  $s_{\infty}^{(\alpha)}$  the GGE entropy density obtained using Bethe ansatz. For  $\alpha = 1/2$ , large finite-size effects are present, and the data start becoming compatible with the asymptotic behaviour (92) only for  $\ell \gtrsim 7$ . On the other hand, for  $\alpha = \infty$ , the data perfectly agree with (92) already for  $\ell \geq 5$ .

## 7. Conclusions

We presented a systematic study of the Rényi entropy after a quantum quench in the XXZ spin-chain starting from the Néel state. We employed a recently developed variation [68] of the quench action method [73, 74] which provides the diagonal and GGE Rényi entropies as generalised free energy on a saddle point macrostate which is different from the one for local observables and von Neumann entropy. As first step we wrote explicit TBA equations (39) (or equivalently (41)) for the root densities describing the macrostate. We did not manage to solve these equations analytically (while for  $\alpha = 1$  it is possible [91]) and so we mainly based our analysis on their exact numerical solution. Plugging these solutions in the saddle-point expectation (46), we readily obtain

the Rényi entropies for arbitrary order  $\alpha$  and anisotropy  $\Delta \geq 1$ . An interesting first observation is that the integrated functions for the Rényi entropy ( $(-\alpha\epsilon_n + s_n)$  in (46)) are not positive for all  $\lambda$ , although  $S_d^{(\alpha)} > 0$ . Thus these quantities cannot be interpreted as the contribution of the quasiparticle  $n$  of momentum  $\lambda$  to the entropy, which must be positive. However, one can think of adding to (46) some functions  $r_n(\lambda)$  such that  $\sum \int_0^{\pi/2} d\lambda r_n(\lambda) = 0$ ; this addition does not change the result for  $S_d^{(\alpha)}$ , but alters the densities.

There are few limits in which the TBA equations can be solved analytically. These serve as reference points for the numerical solutions and they provide very important insights about the overall structure of the solutions themselves. The first limit we consider is the one for large  $\Delta$  which provides a systematic expansion in powers of  $\Delta^{-1}$  for arbitrary  $\alpha$ . For  $\Delta = \infty$  all entropies tend to zero, reflecting the fact that for  $\Delta = \infty$  the Néel state is the ground-state of the XXZ chain. The other limits in which we work out the entire solution correspond to specific values of  $\alpha = 0, 1, \infty$  (which are the max, the von Neumann, and min entropy respectively). While the results for  $\alpha = 0$  and  $\alpha = 1$  have been known by other means and only represent consistency checks for the general approach, the results for  $\alpha = \infty$  are new and insightful. From the definition (5), the min diagonal entropy is determined by the eigenstate with the largest Néel overlap. For  $\Delta > \Delta^*$  this is the ground state of the XXZ chain, while for  $\Delta < \Delta^*$  the min entropy is determined by a finite energy density excited state that we calculate. The transition between these two regimes happens at a special value of anisotropy  $\Delta^* \approx 1.76692$ . In both regimes the min entropy is determined by a state with zero Yang-Yang entropy. However, an important difference is that at small  $\Delta$  the macrostate contains bound-states with an arbitrary number of particles, but for  $\Delta > \Delta^*$  only one-strings are present. We do not expect the relation between the min entropy and the ground state of the XXZ model to be true for other initial states, because this follows from Néel state being the ground-state for large  $\Delta$ . Conversely, the fact that the min entropy is determined by a state with zero Yang-Yang entropy might be generic. This aspect deserves further investigation and could remain true in non-integrable models.

We numerically test our results by constructing explicitly the diagonal ensemble for finite-size XXZ chains. We use both exact (full) diagonalisation and a numerical Monte Carlo implementation [93] of the Bethe ansatz based on the exact formulas [78, 91] for the overlaps with the Néel state. Extrapolating the results to the thermodynamic limit (carefully accounting for finite size effects), we find that the numerical data perfectly match the TBA predictions.

We investigated the relation between the diagonal/GGE entropies and the entanglement Rényi entropies. The latter are obtained using time-dependent Density Matrix Renormalisation Group simulations. Our results confirm that for any  $\alpha$  the entanglement Rényi entropy density is compatible with the density of the thermodynamic entropy obtained by TBA. This result however is not sufficient to permit the reconstruction of the full-time dynamics of the Rényi entropies, as done for the von Neumann entropy [56], by applying the semiclassical picture of Ref. [71]. The bottleneck

in this reasoning is that the thermodynamic entropies are not written in terms of the saddle point root densities describing local observables and only the latter densities correspond to the quasiparticles with a semiclassical dynamics.

It is highly desirable to extend our analysis to quenches from different initial states that can be solved by means of quench action and Bethe ansatz, such as the Majumdar-Ghosh state, the tilted Néel state, and the tilted ferromagnet. The extension to these states should allow to clarify which aspects found here are general and which ones are instead specific of the Néel quench.

Another interesting research direction would be to use the results for the Rényi entanglement entropies to derive the distribution of the entanglement spectrum levels in the steady state, as it has been done at equilibrium in Refs. [52, 125]. In contrast with equilibrium, the structure of the entanglement spectrum after quantum quenches has not been investigated in detail, although some results are already available [126–129]. This calculation requires the knowledge of the analytical dependence on  $\alpha$  of the Rényi entropies, which, although it is not expected to be simple for out-of-equilibrium systems, it should be obtainable in some limits, for instance at large  $\Delta$  and for some specific initial states.

## 8. Acknowledgments

VA acknowledges support from the European Union's Horizon 2020 under the Marie Skłodowska-Curie grant agreement No 702612 OEMBS.

## Appendix A. The diagonal entropy is half of the Yang-Yang entropy

In Ref. [68] it has been shown in very general terms that the diagonal entropy is half of the Yang-Yang entropy, i.e. that in the limit  $\alpha \rightarrow 1$

$$\lim_{\alpha \rightarrow 1} S_d^{(\alpha)} = S_d \equiv -\text{Tr} \rho_d \ln \rho_d = -\frac{1}{2} S_{YY}. \quad (\text{A.1})$$

It is not so straightforward to recover this results from the overlap TBA equation, but it is possible, as we show in this appendix.

The strategy is to consider small deviations of the root densities  $\rho_n$  and  $\eta_n$  around their values at  $\alpha = 1$ . For  $\alpha \rightarrow 1$ , we can write  $\eta_n$  as

$$\eta_n = \eta_n^{(0)} + \eta'_n, \quad \text{with } \eta'_n \ll \eta_n^{(0)}, \quad (\text{A.2})$$

where  $\eta_n^{(0)}$  are the solutions of the TBA equations for  $\alpha = 1$  and  $\eta'_n$  is a  $\mathcal{O}(\alpha - 1)$  correction. Plugging (A.2) into (41), and keeping linear terms in  $\eta'_n$ , one obtains the infinite system of equations

$$\frac{\eta'_n}{\eta_n^{(0)}} = (\alpha - 1)d_n + s \star \left[ \frac{\eta'_{n-1}}{1 + \eta_{n-1}^{(0)}} + \frac{\eta'_{n+1}}{1 + \eta_{n+1}^{(0)}} \right]. \quad (\text{A.3})$$

We now move to the densities  $\rho_n$  and we use the ansatz

$$\rho_n = \rho_n^{(0)} + \rho'_n \quad \text{with } \rho'_n \ll \rho_n^{(0)}. \quad (\text{A.4})$$

Plugging (A.4) in (20) and keeping the leading order in  $\rho'$ , one obtains

$$\rho_n^{(0)}\eta'_n + \rho'_n(1 + \eta_n^{(0)}) = - \sum_m a_{n,m} \star \rho'_m. \quad (\text{A.5})$$

In deriving (A.5) we used that the constraint on the magnetisation  $\sum_m m \int d\lambda \rho_m = 1/2$  implies

$$\sum_m m \int_{-\pi/2}^{\pi/2} d\lambda \rho'_m(\lambda) = 0, \quad (\text{A.6})$$

because  $\sum_m m \int d\lambda \rho_m^{(0)} = 1/2$ . This allows to neglect the term with the magnetic field in (20).

We are finally ready to consider the diagonal entropies (6), writing for  $\alpha \rightarrow 1$

$$\mathcal{E} = \mathcal{E}^{(0)} + \mathcal{E}' \quad (\text{A.7})$$

$$S_{YY} = S_{YY}^{(0)} + S'_{YY}, \quad (\text{A.8})$$

where  $\mathcal{E}'$  and  $S'_{YY}$  are  $\mathcal{O}(\alpha - 1)$ . Plugging in the definitions of  $\mathcal{E}$  and  $S_{YY}$  Eqs. (A.2) and (A.4), it is straightforward to derive that

$$\mathcal{E}' = \frac{L}{2} \sum_n \int_0^{\pi/2} d\lambda \rho'_n(\lambda) g_n, \quad (\text{A.9})$$

$$S'_{YY} = L \sum_n \int_{-\pi/2}^{\pi/2} d\lambda [(\rho_n \eta'_n + \eta_n \rho'_n) \ln(1 + \eta_n^{-1}) + \rho'_n \ln(1 + \eta_n)]. \quad (\text{A.10})$$

Let us now multiply (A.5) by  $\ln(1 + \eta_n^{-1})$ , take the sum over  $n$  and integrate over the rapidity, to obtain

$$\begin{aligned} \sum_n \int_0^{\pi/2} d\lambda [(\rho_n \eta'_n + \eta_n \rho'_n) \ln(1 + \eta_n^{-1}) + \rho'_n \ln(1 + \eta_n^{-1})] \\ = \sum_{m,n} \int_0^{\pi/2} d\lambda d\mu \ln(1 + \eta_n^{-1}(\lambda)) (a_{nm}(\lambda - \mu) + a_{nm}(\lambda + \mu)) \rho'_m(\mu). \end{aligned} \quad (\text{A.11})$$

Similarly, multiplying (39) by  $\rho'_n$  for  $\alpha = 1$ , summing over  $n$  and integrating over  $\lambda$ , one obtains

$$\begin{aligned} \sum_n \int_0^{\pi/2} d\lambda [\ln(\eta_n) - g_n] \rho'_n(\lambda) = \\ = - \sum_{m,n} \int_0^{\pi/2} d\lambda d\mu \ln(1 + \eta_n^{-1}(\mu)) (a_{nm}(\lambda - \mu) + a_{nm}(\lambda + \mu)) \rho'_m(\lambda). \end{aligned} \quad (\text{A.12})$$

The right-hand-side of (A.12), coincides with minus the right-hand side in (A.11), because  $a_{nm}(\lambda - \mu) = a_{nm}(\mu - \lambda)$ . Thus summing (A.11) and (A.12) we have

$$-2\mathcal{E}' + \frac{1}{2}S'_{YY} = 0. \quad (\text{A.14})$$

We finally have

$$-2\alpha\mathcal{E} + \frac{1}{2}S_{YY} \approx -2\mathcal{E}^{(0)} + \frac{1}{2}S_{YY}^{(0)} - 2\mathcal{E}' + \frac{1}{2}S'_{YY} - 2(\alpha - 1)\mathcal{E}^{(0)} = -2(\alpha - 1)\mathcal{E}^{(0)}, \quad (\text{A.15})$$



where in the last step we used (A.14) and (45). This is equivalent to

$$\lim_{\alpha \rightarrow 1} S_d^{(\alpha)} = S_d = \frac{1}{2} S_{YY} \quad (\text{A.16})$$

A fundamental consequence of this equation is that the diagonal entropy  $S_d$  is determined by the saddle point at  $\alpha = 1$ , which describes local and quasilocal observables in the steady state after the quench. This is just a consequence of the fact that the logarithm in the definition of  $S_d$  (A.1) cannot shift the saddle point of the TBA.

## References

- [1] T. Kinoshita, T. Wenger, and D. S. Weiss, A quantum Newton cradle, *Nature* **440**, 900 (2006).
- [2] S. Hofferberth, I. Lesanovsky, B. Fischer, T. Schumm, and J. Schmiedmayer, Non-equilibrium coherence dynamics in one-dimensional Bose gases, *Nature* **449**, 324 (2007).
- [3] S. Trotzky, Y.-A. Chen, A. Flesch, I. P. McCulloch, U. Schollwöck, J. Eisert, and I. Bloch, Probing the relaxation towards equilibrium in an isolated strongly correlated 1D Bose gas, *Nature Phys.* **8**, 325 (2012).
- [4] M. Gring, M. Kuhnert, T. Langen, T. Kitagawa, B. Rauer, M. Schreitl, I. Mazets, D. A. Smith, E. Demler, and J. Schmiedmayer, Relaxation Dynamics and Pre-thermalization in an Isolated Quantum System, *Science* **337**, 1318 (2012).
- [5] M. Cheneau, P. Barmettler, D. Poletti, M. Endres, P. Schaua, T. Fukuhara, C. Gross, I. Bloch, C. Kollath, and S. Kuhr, Light-cone-like spreading of correlations in a quantum many-body system, *Nature* **481**, 484 (2012).
- [6] T. Langen, R. Geiger, M. Kuhnert, B. Rauer, and J. Schmiedmayer, Local emergence of thermal correlations in an isolated quantum many-body system, *Nature Phys.* **9**, 640 (2013).
- [7] T. Fukuhara, A. Kantian, M. Endres, M. Cheneau, P. Schaua, S. Hild, C. Gross, U. Schollwöck, T. Giamarchi, I. Bloch, and S. Kuhr, *Nature Phys.* **9**, 235 (2013).
- [8] T. Langen, S. Erne, R. Geiger, B. Rauer, T. Schweigier, M. Kuhnert, W. Rohringer, I. E. Mazets, T. Gasenzer, J. Schmiedmayer, Experimental observation of a generalized Gibbs ensemble, *Science* **348**, 207 (2015).
- [9] T. Langen, T. Gasenzer, and J. Schmiedmayer, Prethermalization and universal dynamics in near-integrable quantum systems, *J. Stat. Mech.* (2016) 064009.
- [10] A. M. Kaufman, M. E. Tai, A. Lukin, M. Rispoli, R. Schittko, P. M. Preiss, and M. Greiner, Quantum thermalization through entanglement in an isolated many-body system, *Science* **353**, 794 (2016).
- [11] J. von Neumann, Beweis des Ergodensatzes und des H-Theorems, *Z Phys.* **57**, 30 (1929).
- [12] R. V. Jensen and R. Shankar, Statistical behaviour in Deterministic Quantum Systems with Few Degrees of Freedom, *Phys. Rev. Lett.* **54**, 1879 (1985).
- [13] J. M. Deutsch, Quantum statistical mechanics in a closed system, *Phys. Rev. A* **43**, 2046 (1991).
- [14] M. Srednicki, Chaos and quantum thermalization, *Phys. Rev. E* **50**, 888 (1994).
- [15] M. Rigol, V. Dunjko, and M. Olshanii, Thermalization and its mechanism for generic isolated quantum systems, *Nature* **452**, 854 (2008).
- [16] M. Rigol and M. Srednicki, Alternatives to Eigenstate Thermalization, *Phys. Rev. Lett.* **108**, 110601 (2012).
- [17] L. D'Alessio, Y. Kafri, A. Polkovnikov, and M. Rigol, From Quantum Chaos and Eigenstate Thermalization to Statistical Mechanics and Thermodynamics, *Adv. Phys.* **65**, 239 (2016).
- [18] M. Rigol, V. Dunjko, V. Yurovsky, and M. Olshanii, Relaxation in a Completely Integrable Many-Body Quantum System: An *Ab Initio* Study of the Dynamics of the Highly Excited States of 1D Lattice Hard-Core Bosons. *Phys. Rev. Lett.* **98**, 050405 (2007).
- [19] M. A. Cazalilla, Effect of Suddenly Turning on Interactions in the Luttinger Model, *Phys. Rev. Lett.* **97**, 156403 (2006).



- [20] T. Barthel and U. Schollwöck, Dephasing and the Steady State in Quantum Many-Particle Systems. *Phys. Rev. Lett.* **100**, 100601 (2008).
- [21] M. Cramer, C. M. Dawson, J. Eisert, and T. J. Osborne, Exact Relaxation in a Class of Nonequilibrium Quantum Lattice Systems, *Phys. Rev. Lett.* **100**, 030602 (2008).
- [22] M. Cramer and J. Eisert, A quantum central limit theorem for non-equilibrium systems: exact local relaxation of correlated states, *New J. Phys.* **12**, 055020 (2010).
- [23] M. Fagotti and P. Calabrese, Evolution of entanglement entropy following a quantum quench: Analytic results for the XY chain in a transverse magnetic field. *Phys. Rev. A* **78**, 010306 (2008).
- [24] M. A. Cazalilla, A. Iucci, and M.-C. Chung, Thermalization and quantum correlations in exactly solvable models, *Phys. Rev. E* **85**, 011133 (2012).
- [25] P. Calabrese, F. H. L. Essler, and M. Fagotti, Quantum Quench in the Transverse-Field Ising Chain, *Phys. Rev. Lett.* **106**, 227203 (2011);  
P. Calabrese, F. H. L. Essler, and M. Fagotti, Quantum quench in the transverse field Ising chain: I. Time evolution of order parameter correlators, *J. Stat. Mech.* (2012) P07016.
- [26] P. Calabrese, F. H. L. Essler, and M. Fagotti, Quantum quenches in the transverse field Ising chain: II. Stationary state properties, *J. Stat. Mech.* (2012) P07022.
- [27] J. Mossel and J.-S. Caux, Generalized TBA and generalized Gibbs, *J. Phys. A* **45**, 255001 (2012).
- [28] D. Fioretto and G. Mussardo, Quantum quenches in integrable field theories, *New J. Phys.* **12**, 055015 (2010);  
S. Sotiriadis, D. Fioretto, and G. Mussardo, Zamolodchikov-Faddeev algebra and quantum quenches in integrable field theories, *J. Stat. Mech.* (2012) P02017.
- [29] M. Collura, S. Sotiriadis, and P. Calabrese, Equilibration of a Tonks-Girardeau Gas Following a Trap Release, *Phys. Rev. Lett.* **110**, 245301 (2013);  
M. Collura, S. Sotiriadis, and P. Calabrese, Quench dynamics of a Tonks-Girardeau gas released from a harmonic trap, *J. Stat. Mech.* (2013) P09025.
- [30] M. Fagotti and F. H. L. Essler, Stationary behaviour of observables after a quantum quench in the spin-1/2 Heisenberg XXZ chain, *J. Stat. Mech.* (2013) P07012.
- [31] B. Pozsgay, The generalized Gibbs ensemble for Heisenberg spin chains, *J. Stat. Mech.* P07003 (2013).
- [32] M. Fagotti and F. H. L. Essler, Reduced Density Matrix after a Quantum Quench, *Phys. Rev. B* **87**, 245107 (2013).
- [33] M. Kormos, M. Collura, and P. Calabrese, Analytic results for a quantum quench from free to hard-core one-dimensional bosons, *Phys. Rev. A* **89**, 013609 (2014).
- [34] S. Sotiriadis and P. Calabrese, Validity of the GGE for quantum quenches from interacting to noninteracting models, *J. Stat. Mech.* (2014) P07024.
- [35] M. Fagotti, M. Collura, F. H. L. Essler, and P. Calabrese, Relaxation after quantum quenches in the spin-1/2 Heisenberg XXZ chain, *Phys. Rev. B* **89**, 125101 (2014).
- [36] E. Ilievski, J. De Nardis, B. Wouters, J.-S. Caux, F. H. L. Essler, and T. Prosen, Complete Generalized Gibbs Ensembles in an Interacting Theory, *Phys. Rev. Lett.* **115**, 157201 (2015);  
E. Ilievski, E. Quinn, J. D. Nardis, and M. Brockmann, String-charge duality in integrable lattice models, *J. Stat. Mech.* (2016) 063101.
- [37] V. Alba, Simulating the Generalized Gibbs Ensemble (GGE): a Hilbert space Monte Carlo approach. [arXiv:1507.06994](https://arxiv.org/abs/1507.06994).
- [38] T. Langen, S. Erne, R. Geiger, B. Rauer, T. Schweigler, M. Kuhnert, W. Rohringer, I. E. Mazets, T. Gasenzer, and J. Schmiedmayer, Experimental observation of a generalized Gibbs ensemble, *Science* **348**, 207 (2015).
- [39] F. H. L. Essler, G. Mussardo, and M. Panfil, Generalized Gibbs ensembles for quantum field theories, *Phys. Rev. A* **91**, 051602 (2015);  
F. H. L. Essler, G. Mussardo, and M. Panfil, On Truncated Generalized Gibbs Ensembles in the Ising Field Theory, *J. Stat. Mech.* (2017) 013103.

- [40] J. Cardy, Quantum quenches to a critical point in one dimension: some further results, *J. Stat. Mech.* (2016) 023103.
- [41] S. Sotiriadis, Memory-preserving equilibration after a quantum quench in a 1d critical model, *Phys. Rev. A* **94**, 031605 (2016).
- [42] A. Bastianello and S. Sotiriadis, Quasi locality of the GGE in interacting-to-free quenches in relativistic field theories, *J. Stat. Mech.* (2017) 023105.
- [43] E. Vernier and A. Cortés Cubero, Quasilocal charges and the complete GGE for field theories with non diagonal scattering, *J. Stat. Mech.* (2017) 23101.
- [44] B. Pozsgay, E. Vernier, and M. A. Werner, On Generalized Gibbs Ensembles with an infinite set of conserved charges, [arXiv:1703.09516](#) (2017).
- [45] L. Vidmar and M. Rigol, Generalized Gibbs ensemble in integrable lattice models, *J. Stat. Mech.* (2016) 064007.
- [46] C. Gogolin and J. Eisert, Equilibration, thermalisation, and the emergence of statistical mechanics in closed quantum systems, *Rep. Prog. Phys.* **79**, 056001 (2016).
- [47] P. Calabrese, F. H. L. Essler, and G. Mussardo, Introduction to “Quantum Integrability in Out of Equilibrium Systems”, *J. Stat. Mech.* (2016) P064001.
- [48] F. H. L. Essler and M. Fagotti, Quench dynamics and relaxation in isolated integrable quantum spin chains, *J. Stat. Mech.* (2016) 064002.
- [49] B. Pozsgay and V. Eisler, Real-time dynamics in a strongly interacting bosonic hopping model: Global quenches and mapping to the XX chain, *J. Stat. Mech.* (2016) 053107.
- [50] E. Ilievski, M. Mednjak, T. Prosen, and L. Zadnik, Quasilocal charges in integrable lattice systems, *J. Stat. Mech.* (2016) P064008.
- [51] P. Calabrese, J. Cardy, and B. Doyon, Entanglement entropy in extended quantum systems, *J. Phys. A* **42** 500301 (2009);  
N. Laflorencie, Quantum entanglement in condensed matter systems, *Physics Report* **643**, 1 (2016).
- [52] P. Calabrese and A. Lefevre, Entanglement spectrum in one dimensional systems, *Phys. Rev. A* **78**, 032329 (2008).
- [53] P. Calabrese and J. Cardy, Entanglement entropy and quantum field theory, *J. Stat. Mech.* P06002 (2004);  
P. Calabrese and J. Cardy, Entanglement entropy and conformal field theory, *J. Phys. A* **42**, 504005 (2009).
- [54] M. Caraglio and F. Gliozzi, Entanglement entropy and twist fields, *JHEP* 0811: 076 (2008);  
M. B. Hastings, I. Gonzalez, A. B. Kallin, and R. G. Melko, Measuring Renyi Entanglement Entropy with Quantum Monte Carlo, *Phys. Rev. Lett.* **104**, 157201 (2010).;  
C.-M. Chung, L. Bonnes, P. Chen, and A. M. Lauchli, Entanglement Spectroscopy using Quantum Monte Carlo, *Phys. Rev. B* **89**, 195147 (2014).
- [55] R. Islam, R. Ma, P. M. Preiss, M. E. Tai, A. Lukin, M. Rispoli, and M. Greiner, Measuring entanglement entropy in a quantum many-body system, *Nature* **528**, 77 (2015).
- [56] V. Alba and P. Calabrese, Entanglement and thermodynamics after a quantum quench in integrable systems, *PNAS* **114**, 7947 (2017).
- [57] A. Polkovnikov, Microscopic diagonal entropy and its connection to basic thermodynamic relations, *Ann. Phys.* **326**, 486 (2011).
- [58] L. F. Santos, A. Polkovnikov, and M. Rigol, Entropy of isolated quantum systems after a quench, *Phys. Rev. Lett.* **107**, 040601 (2011).
- [59] L. F. Santos, A. Polkovnikov, and M. Rigol, Weak and strong typicality in quantum systems, *Phys. Rev. E* **86**, 010102 (2012).
- [60] V. Gurarie, Global large time dynamics and the generalized Gibbs ensemble, *J. Stat. Mech.* (2013) P02014.
- [61] M. Fagotti, Finite-size corrections vs. relaxation after a sudden quench, *Phys. Rev. B* **87**, 165106 (2013).

- [62] J. M. Deutsch, H. Li, and A. Sharma, Microscopic origin of thermodynamic entropy in isolated systems, *Phys. Rev. E* **87**, 042135 (2013).
- [63] M. Collura, M. Kormos, and P. Calabrese, Stationary entropies following an interaction quench in 1D Bose gas, *J. Stat. Mech.* P01009 (2014).
- [64] B. Dóra, Escort distribution function of work done and diagonal entropies in quenched Luttinger liquids, *Phys. Rev. B* **90**, 245132 (2014).
- [65] M. Kormos, L. BucciAntini, and P. Calabrese, Stationary entropies after a quench from excited states in the Ising chain, *EPL* **107**, 40002 (2014);  
L. BucciAntini, M. Kormos, and P. Calabrese, Quantum quenches from excited states in the Ising chain, *J. Phys. A* **47**, 175002 (2014).
- [66] W. Beugeling, A. Andreanov, and M. Haque, Global characteristics of all eigenstates of local many-body Hamiltonians: participation ratio and entanglement entropy, *J. Stat. Mech.* (2015) P02002.
- [67] L. Piroli, E. Vernier, P. Calabrese, and M. Rigol, Correlations and diagonal entropies after quantum quenches in XXZ chains, *Phys. Rev. B* **95**, 054308 (2017).
- [68] V. Alba and P. Calabrese, Quench action and Renyi entropies in integrable systems, [arXiv:1705.10765](https://arxiv.org/abs/1705.10765).
- [69] B. Bertini, E. Tartaglia, and P. Calabrese, Quantum Quench in the Infinitely Repulsive Hubbard Model: The Stationary State, [arXiv:1707.01073](https://arxiv.org/abs/1707.01073).
- [70] G. Delfino, Quantum quenches with integrable pre-quench dynamics, *J. Phys. A* **47** (2014) 402001.
- [71] P. Calabrese and J. Cardy, Evolution of Entanglement Entropy in One-Dimensional Systems, *J. Stat. Mech.* (2005) P04010.
- [72] P. Calabrese and J. Cardy, Quantum quenches in 1+1 dimensional conformal field theories, *J. Stat. Mech.* (2016) 064003.
- [73] J.-S. Caux and F. H. L. Essler, Time evolution of local observables after quenching to an integrable model, *Phys. Rev. Lett.* **110**, 257203 (2013).
- [74] J.-S. Caux, The Quench Action, *J. Stat. Mech.* (2016) 064006.
- [75] C. N. Yang and C. P. Yang, Thermodynamics of a One Dimensional System of Bosons with Repulsive Delta Function Interaction, *J. Math. Phys.* **10**, 1115 (1969).
- [76] V. Gritsev, T. Rostunov, and E. Demler, Exact methods in the analysis of the non-equilibrium dynamics of integrable models: application to the study of correlation functions for non-equilibrium 1D Bose gas, *J. Stat. Mech.* (2010) P05012.
- [77] P. Le Doussal and P. Calabrese, The KPZ equation with flat initial condition and the directed polymer with one free end *J. Stat. Mech.* (2012) P06001;  
P. Calabrese and P. Le Doussal, Interaction quench in a Lieb-Liniger model and the KPZ equation with flat initial conditions *J. Stat. Mech.* (2014) P05004.
- [78] B. Pozsgay, Overlaps between eigenstates of the XXZ spin-1/2 chain and a class of simple product states, *J. Stat. Mech.* (2014) P06011.
- [79] J. De Nardis, B. Wouters, M. Brockmann, and J.-S. Caux, Solution for an interaction quench in the Lieb-Liniger Bose gas, *Phys. Rev. A* **89**, 033601 (2014).
- [80] M. Brockmann, J. D. Nardis, B. Wouters, and J.-S. Caux, A Gaudin-like determinant for overlaps of Néel and XXZ Bethe states, *J. Phys. A* **47**, 145003 (2014);  
M. Brockmann, Overlaps of q-raised Néel states with XXZ Bethe states and their relation to the Lieb-Liniger Bose gas, *J. Stat. Mech.* (2014) P05006;  
M. Brockmann, J. De Nardis, B. Wouters, and J.-S. Caux, Néel-XXZ state overlaps: odd particle numbers and Lieb-Liniger scaling limit, *J. Phys. A* **47**, 345003 (2014).
- [81] L. Piroli and P. Calabrese, Recursive formulas for the overlaps between Bethe states and product states in XXZ Heisenberg chains, *J. Phys. A* **47**, 385003 (2014).
- [82] M. de Leeuw, C. Kristjansen, and K. Zarembo, One-point Functions in Defect CFT and Integrability, *JHEP* **08** (2015) 098;  
I. Buhl-Mortensen, M. de Leeuw, C. Kristjansen, and K. Zarembo, One-point Functions in

- AdS/dCFT from Matrix Product States, [JHEP 02 \(2016\) 052](#);  
O. Foda and K. Zarembo, Overlaps of partial Néel states and Bethe states, [J. Stat. Mech. \(2016\) 23107](#).
- [83] M. de Leeuw, C. Kristjansen, and S. Mori, AdS/dCFT one-point functions of the SU(3) sector, [Phys. Lett. B 763, 197 \(2016\)](#).
- [84] D. X. Horváth, S. Sotiriadis, and G. Takács, Initial states in integrable quantum field theory quenches from an integral equation hierarchy, [Nucl. Phys. B 902, 508 \(2016\)](#);  
D. X. Horváth and G. Takács, Overlaps after quantum quenches in the sine-Gordon model, [Phys. Lett. B 771, 539 \(2017\)](#).
- [85] P. P. Mazza, J.-M. Stéphan, E. Canovi, V. Alba, M. Brockmann, and M. Haque, Overlap distributions for quantum quenches in the anisotropic Heisenberg chain, [J. Stat. Mech. \(2016\) 013104](#).
- [86] J. R. Garrison and T. Grover, Does a single eigenstate encode the full Hamiltonian?, [arXiv:1503.00729](#).
- [87] M. Takahashi, *Thermodynamics of one-dimensional solvable models*, Cambridge University Press, Cambridge, 1999.
- [88] B. Bertini, D. Schuricht, and F. H. L. Essler, Quantum quench in the sine-Gordon model, [J. Stat. Mech. \(2014\) P10035](#).
- [89] B. Bertini, L. Piroli, and P. Calabrese, Quantum quenches in the sinh-Gordon model: steady state and one-point correlation functions, [J. Stat. Mech. \(2016\) 063102](#).
- [90] B. Pozsgay, The dynamical free energy and the Loschmidt echo for a class of quantum quenches in the Heisenberg spin chain, [J. Stat. Mech. \(2013\) P10028](#).
- [91] B. Wouters, J. De Nardis, M. Brockmann, D. Fioretto, M. Rigol, and J.-S. Caux, Quenching the Anisotropic Heisenberg Chain: Exact Solution and Generalized Gibbs Ensemble Predictions, [Phys. Rev. Lett. 113, 117202 \(2014\)](#);  
M. Brockmann, B. Wouters, D. Fioretto, J. D. Nardis, R. Vlijm, and J.-S. Caux, Quench action approach for releasing the Néel state into the spin-1/2 XXZ chain, [J. Stat. Mech. \(2014\) P12009](#).
- [92] B. Pozsgay, M. Mestyán, M. A. Werner, M. Kormos, G. Zaránd, and G. Takács, Correlations after Quantum Quenches in the XXZ Spin Chain: Failure of the Generalized Gibbs Ensemble, [Phys. Rev. Lett. 113, 117203 \(2014\)](#);  
M. Mestyán, B. Pozsgay, G. Takács, and M. A. Werner, Quenching the XXZ spin chain: quench action approach versus generalized Gibbs ensemble, [J. Stat. Mech. \(2015\) P04001](#).
- [93] V. Alba, and P. Calabrese, The quench action approach in finite integrable spin chains, [J. Stat. Mech. \(2016\), 043105](#).
- [94] L. Piroli, B. Pozsgay, and E. Vernier, From the quantum transfer matrix to the quench action: the Loschmidt echo in XXZ Heisenberg spin chains, [J. Stat. Mech. \(2017\) 23106](#).
- [95] M. Mestyán, B. Bertini, L. Piroli, and P. Calabrese, Exact solution for the quench dynamics of a nested integrable system, [J. Stat. Mech. \(2017\) 083103](#).
- [96] L. Piroli, P. Calabrese, and F. H. L. Essler, Multiparticle Bound-State Formation following a Quantum Quench to the One-Dimensional Bose Gas with Attractive Interactions, [Phys. Rev. Lett. 116, 070408 \(2016\)](#);  
L. Piroli, P. Calabrese, and F. H. L. Essler, Quantum quenches to the attractive one-dimensional Bose gas: exact results, [SciPost Phys. 1, 001 \(2016\)](#).
- [97] L. Bucciantini, Stationary State After a Quench to the Lieb-Liniger from Rotating BECs, [J Stat Phys 164, 621 \(2016\)](#).
- [98] J. De Nardis, M. Panfil, A. Gambassi, L. F. Cugliandolo, R. Konik, and L. Foini, Probing non-thermal density fluctuations in the one-dimensional Bose gas, [arXiv:1704.06649](#);  
J. De Nardis and M. Panfil, Exact correlations in the Lieb-Liniger model and detailed balance out-of-equilibrium, [SciPost Phys. 1, 015 \(2016\)](#).
- [99] L. Piroli, E. Vernier, and P. Calabrese, Exact steady states for quantum quenches in integrable Heisenberg spin chains, [Phys. Rev. B 94, 054313 \(2016\)](#).

- [100] J. De Nardis and J.-S. Caux, Analytical expression for a post-quench time evolution of the one-body density matrix of one-dimensional hard-core bosons, *J. Stat. Mech.* (2014), P12012.
- [101] J. De Nardis, L. Piroli, and J.-S. Caux, Relaxation dynamics of local observables in integrable systems, *J. Phys. A* **48**, 43FT01 (2015).
- [102] L. Piroli and P. Calabrese, Exact dynamics following an interaction quench in a one-dimensional anyonic gas, *Phys. Rev. A* **96**, 023611 (2017).
- [103] R. Orús, J. I. Latorre, J. Eisert, and M. Cramer, Half the entanglement in critical systems is distillable from a single specimen, *Phys. Rev. A* **73**, 060303(R) (2006).
- [104] A. W. Sandvik, Computational Studies of Quantum Spin Systems, *AIP Conference Proceedings* **1297**, 135 (2010).
- [105] S. R. White and A. E. Feiguin, Real-Time Evolution Using the Density Matrix Renormalization Group, *Phys. Rev. Lett.* **93**, 076401 (2004).
- [106] A. J. Daley, C. Kollath, U. Schollock, and G. Vidal, Time-dependent density-matrix renormalization-group using adaptive effective Hilbert spaces, *J. Stat. Mech.* (2004) P04005.
- [107] U. Schollwöck, The density-matrix renormalization group, *Rev. Mod. Phys.* **77**, 259 (2005).
- [108] U. Schollwöck, The density-matrix renormalization group in the age of matrix product states, *Annals of Physics* **326**, 96 (2011).
- [109] For the implementation we used the ITENSOR library (<http://itensor.org/>).
- [110] G. De Chiara, S. Montangero, P. Calabrese, and R. Fazio, Entanglement Entropy dynamics in Heisenberg chains, *J. Stat. Mech.* (2006) P03001.
- [111] V. Eisler and I. Peschel, Entanglement in a periodic quench, *Ann. Phys. (Berlin)* **17**, 410 (2008).
- [112] A. Laeuchli and C. Kollath, Spreading of correlations and entanglement after a quench in the Bose-Hubbard model, *J. Stat. Mech.* P05018 (2008).
- [113] H. Kim and D. A. Huse, Ballistic Spreading of Entanglement in a Diffusive Nonintegrable System, *Phys. Rev. Lett.* **111**, 127205 (2013).
- [114] M. G. Nezhadhighi and M. A. Rajabpour, Entanglement dynamics in short and long-range harmonic oscillators, *Phys. Rev. B* **90**, 205438 (2014).
- [115] A. Coser, E. Tonni, and P. Calabrese, Entanglement negativity after a global quantum quench, *J. Stat. Mech.* P12017 (2014).
- [116] M. Collura, P. Calabrese, and F. H. L. Essler, Quantum quench within the gapless phase of the spin-1/2 Heisenberg XXZ spin-chain, *Phys. Rev. B* **92**, 125131 (2015).
- [117] M. Fagotti and M. Collura, Universal prethermalization dynamics of entanglement entropies after a global quench, [arXiv:1507.02678](https://arxiv.org/abs/1507.02678).
- [118] J. S. Cotler, M. P. Hertzberg, M. Mezei, and M. T. Mueller, Entanglement Growth after a Global Quench in Free Scalar Field Theory, *JHEP* **11** (2016) 166.
- [119] A. S. Buyskikh, M. Fagotti, J. Schachenmayer, F. Essler, and A. J. Daley, Entanglement growth and correlation spreading with variable-range interactions in spin and fermionic tunnelling models, *Phys. Rev. A* **93**, 053620 (2016).
- [120] J. Dubail, Entanglement scaling of operators: a conformal field theory approach, with a glimpse of simulability of long-time dynamics in 1+1d, *J. Phys. A* **50**, 234001 (2017).
- [121] M. Kormos, M. Collura, G. Takács, and P. Calabrese, Real time confinement following a quantum quench to a non-integrable model, *Nature Physics* **13**, 246 (2017).
- [122] C. Pascu Moca, M. Kormos, and G. Zarand, Semi-semiclassical theory of quantum quenches in one dimensional systems, [arXiv:1609.00974](https://arxiv.org/abs/1609.00974).
- [123] A. Nahum, J. Ruhman, S. Vijay, and J. Haah, Quantum Entanglement Growth Under Random Unitary Dynamics, *Phys. Rev. X* **7**, 031016 (2017);  
A. Nahum, S. Vijay, and J. Haah, Operator Spreading in Random Unitary Circuits [arXiv:1705.08975](https://arxiv.org/abs/1705.08975).
- [124] E. Bianchi, L. Hackl, and N. Yokomizo, Linear growth of the entanglement entropy and the Kolmogorov-Sinai rate, [arXiv:1709.00427](https://arxiv.org/abs/1709.00427).
- [125] V. Alba, P. Calabrese, and E. Tonni, Entanglement spectrum degeneracy and Cardy formula in

- 1+1 dimensional conformal field theories, [arXiv:1707.07532](#).
- [126] D. Poilblanc, Out-of-equilibrium Correlated Systems: Bipartite Entanglement as a Probe of Thermalization, [Phys. Rev. B](#) **84**, 045120 (2011).
  - [127] G. Torlai, L. Tagliacozzo, and G. De Chiara, Dynamics of the entanglement spectrum in spin chains, [J. Stat. Mech.](#) (2014) P06001.
  - [128] E. Canovi, E. Ercolessi, P. Naldesi, L. Taddia, and D. Vodola, Dynamics of entanglement entropy and entanglement spectrum crossing a quantum phase transition, [Phys. Rev. B](#) **89**, 104303 (2014).
  - [129] Y.-H. Jhu, P. Chen, and M.-C. Chung, Relaxation of the entanglement spectrum in quench dynamics of topological systems, [J. Stat. Mech.](#) (2017) 073105.